DETAILED THIN-BEDDED FACIES ANALYSIS OF MANCOS C IN THE UPPER MANCOS SHALE, NEW MEXICO

By CRISTINA GENOVESE, B.Sc. (Hons.)

A Thesis Submitted to the School of Graduate Studies in Partial Fulfilment of the Requirements for the Degree Master of Science

McMaster University MASTER OF SCIENCE (2017) Hamilton, Ontario (School of Geography and Earth Sciences)

TITLE: Detailed Thin-bedded Facies Analysis of Mancos C in the Upper Mancos Shale, New Mexico

AUTHOR: Cristina Genovese, Honours B.Sc. (McMaster University)

SUPERVISOR: Dr. Janok Bhattacharya

NUMBER OF PAGES: viii: 63

Abstract

Fine grained sediments were common in epicontinental seas, with shallow slopes, such as the Cretaceous Western Interior Seaway. However, proposed mechanisms for offshore mud transport, such as turbidity currents, tempestites, and hyperpycnal flows, require significant slopes. A core from the Upper Mancos Shale, Mancos C, located in the San Juan Basin of New Mexico was analysed to determine the dominant transport processes bringing sediment offshore. A detailed facies analysis was conducted, over 54 m of slabbed core, using sedimentological data, such as grain size, type of sedimentary structures, bed thickness, lithology, clay content, fossils, ichnofacies, and degree of bioturbation. The facies observed in the core show that multiple processes, including ignitive turbidity currents, hypopycnal and hyperpycnal flows, and tempestites, were responsible for the deposition of the Mancos C core. The resuspension of mud on the inner shelf by storm waves also played a key role in moving mud further offshore. Tidal influence within the Mancos C was relatively small.

Acknowledgements

Firstly, I would like to thank my supervisor, Dr. Janok Bhattacharya, for his constant support throughout this project. His advice and guidance has lead me through this project, and I am grateful for all of the field work experiences I have had while being his student.

Thank you to entire McMaster Sedimentology Research Team in New Mexico, especially Matt Leung and Kristen Dosen, who were with me in the core lab. They were willing to answer any questions or concerns I had about this project while in Socorro, New Mexico.

I would also like to thank the staff at the New Mexico Bureau of Geology and Mineral Resources in Socorro, New Mexico, specifically, Ron Broadhead and Annabelle Lopez, for allowing myself and my colleagues to spend around two months in the core lab, and for giving us useful information about shales.

Finally, I would like to thank my family and friends for their endless support throughout my educational career.

I also acknowledge funding from McMaster University Quantitative Sedimentology Laboratories with support from BP and NSERC Discovery Grant RPGIN 05780-14 to Dr. Bhattacharya.

<u>Table of Contents</u>

List of Figures and Tables

1. Introduction

Fine grained sediments were common in ancient large epicontental seas, such as the Cretaceous Western Interior Seaway (Schieber, 2016). These seas had bottom slopes ranging from 0.001-0.005^{o} (absolute values: 1.7 x 10^{-5} to 8.7 x 10^{-5}) (Schieber, 2016). Therefore, it is likely that the proposed mechanisms for offshore mud transport, such as turbidity currents, tempestites, and hyperpycnites, would not have been able to transport sediment far into the Cretaceous Western Interior Seaway (Schieber, 2016). Many of these processes, except hyperpycnal flows, require steeper slopes (>0.1^{o}) for the sustained movement of sediment (figure 1; Schieber, 2016). Because of this, they would only be able to transport fine grained sediments up to 100 kilometers offshore (figure 1; Schieber, 2016). Therefore, it is unlikely that these processes were the main mechanisms responsible for offshore sediment transport. Instead, it is hypothesized that wind and tide induced bottom circulation was the main mechanism spreading muddy sediments across epicontinental seas (Schieber, 2016).

Fine-grained sediments also have the ability to be transported alongshelf. Coriolis forces deflect the flow to the right (northern hemisphere) or left (southern hemisphere) resulting in a geostrophic flow that is capable of moving sediment alongshelf or obliquely across the shelf, creating mud belts extending 1000s of kilometers alongshelf (Duke, 1990; Kineke et al., 1996; Nittrouer et al., 1996; Correggiari et al., 2005; Plint et al., 2012). Alongshelf transport can also affect the ability of processes, such as hyperpycnal flows, turbidity currents, etc., to transport sediment offshore (Khan et al., 2005).

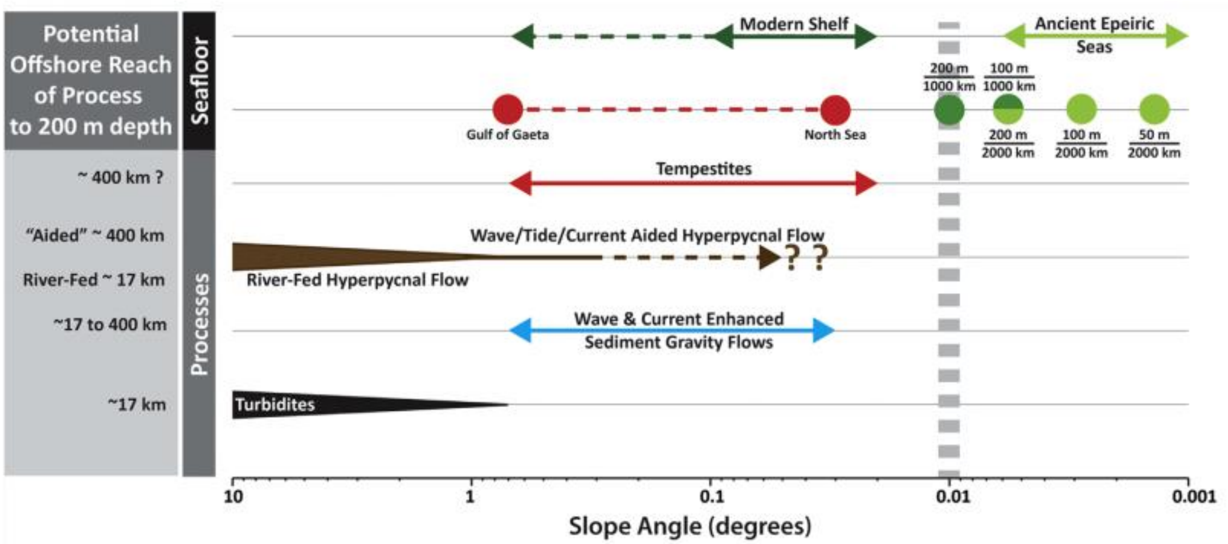

Figure 1: Slope angles and potential offshore reach for depositional processes, such as tempestites, wave/tide/current aided hyperpycnal flow, wave and current enhanced sediment gravity flows, and turbidites (taken from Schieber, 2016).

Objectives

The main objective of this study is to evaluate the vertical facies variability within the Mancos C Shale in New Mexico on a millimeter to centimeter scale. The Mancos C was chosen because it showed the greatest variability of facies throughout the core and it is of interest to oil companies. This study will also evaluate the vertical facies within multiple parasequences throughout the Mancos C to determine the main processes transporting mud offshore and alongshelf, forming these thin beds, and to classify the dominant depositional processes (i.e., wave, tidal, fluvial, or mixed) within a parasequence.

In most studies today, detailed facies analysis of mudstones is done by looking at thin sections (e.g., Macquaker et al., 2010; Plint, 2014). From these studies, millimeter scale facies can be observed, and, with the use of SEMs, micrometer scale mineral composition of clay and silt, and grain orientation can be observed. This study will also attempt to see if the same amount of detail can be observed within a well preserved core.

2. Geologic Setting and Study Area

The Mancos Shale was deposited in the Western Interior Seaway of North America during the Turonian and Coniacian ages (figure 2; Ridgley et al., 2013). The Western Interior Seaway (figure 3) was a vast foreland basin lasting for over 50 myr during the mid-to late Cretaceous (Sageman and Arthur, 1994). At its maximum extent, the basin extended from the Arctic Ocean to the Gulf of Mexico, a distance of 4800 km in the north-south direction, and from Utah to Iowa, a distance of 1600 km in the west-east direction (Sageman and Arthur, 1994). Tethyan waters from the Gulf of Mexico and Boreal waters from the Arctic Ocean both flooded the basin in the Late Albian (He et al., 2005). The seaway lasted until Maastrichtian times (He et al., 2005).

In the San Juan Basin, the Mancos Shale is subdivided into the Lower and the Upper Mancos Shale, which are separated by the basal Niobrara unconformity (figure 4) (Lamb, 1968; Ridgley et al., 2013). The Upper Mancos Shale consists of dark gray, kerogen-rich marine shale that is interbedded with marine siltstones and fine grained sandstones (Broadhead, 2015). Broadhead (2015) recently further subdivided the Upper Mancos Shale into three units: Mancos A, Mancos B and C (figure 4). These subdivisions are based on laterally continuous sand, silt, and carbonate markers seen on gamma ray and resistivity logs (Broadhead, 2015). The Mancos C is 75 to 470 ft thick and thickens towards the northwest (Broadhead, 2015).

This study focuses on sedimentological data obtained from a slabbed core that was drilled in the San Juan Basin, Rio Arriba County of northwestern New Mexico (figure 3). The core, labelled 148 M San Juan 28-6 Unit, was made available by the New Mexico Bureau of Geology and Mineral Resources in Socorro, New Mexico. The analysed portion of the core for this study only includes Mancos C, which has a thickness of approximately 419 ft.

Regional correlations (figure 2) and paleogeographic reconstructions (figure 3) indicate the cored well was located about 137 km (85 miles) from shorelines to the west. Sediment was likely deposited in a water depth of < 100 m, indicating that the slope angle of the San Juan Basin shelf was 0.04 degrees (absolute value: 7×10^{-4}). This angle is an order magnitude higher than predicted slopes for ancient continental seas (e.g., 8.7×10^{-5}), however, it is still quite a shallow slope.

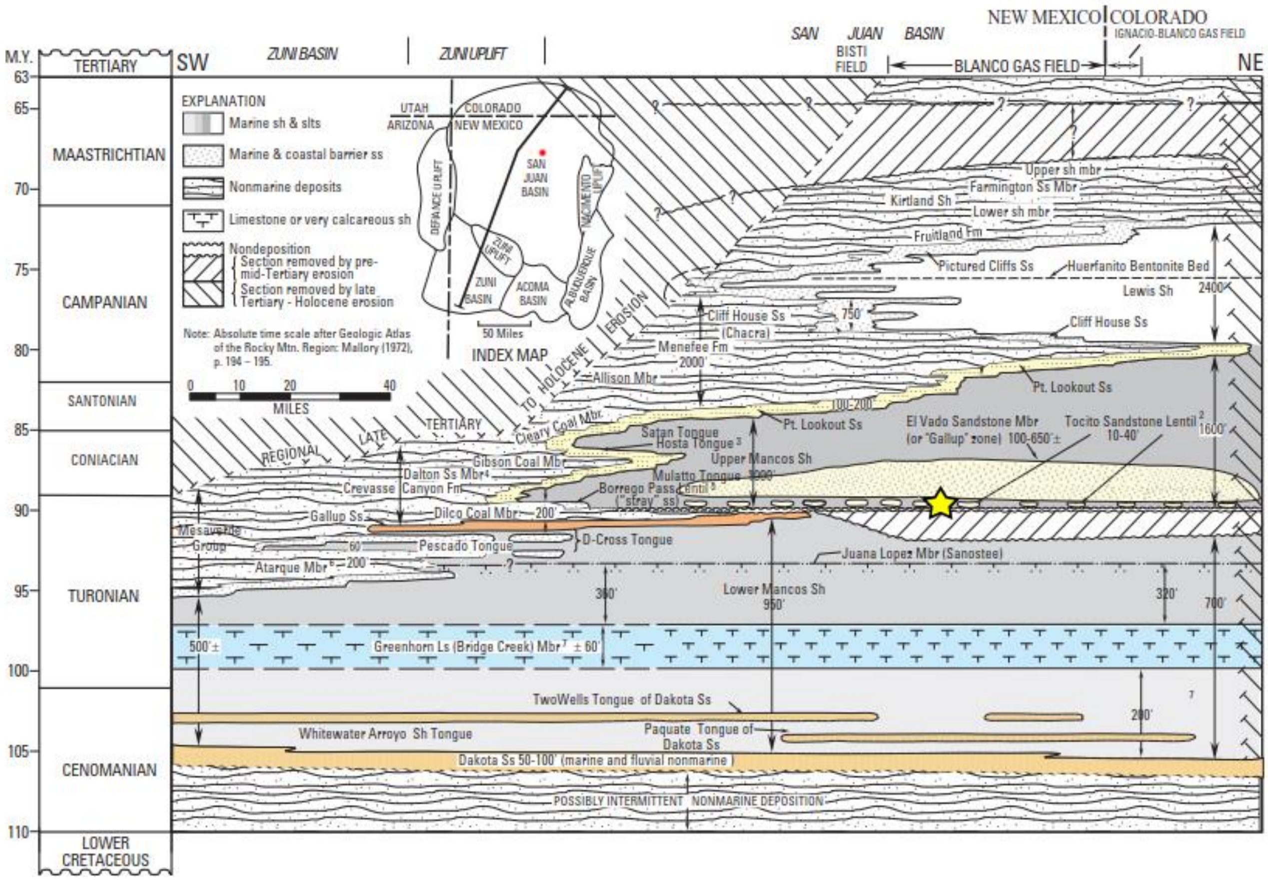

Figure 2: Time-stratigraphic cross section in the San Juan Basin. Location of cored well in Mancos C of the Upper Mancos Shale is represented by red dot on the index map, and a yellow star on cross section (taken from Ridgley et al., 2013).

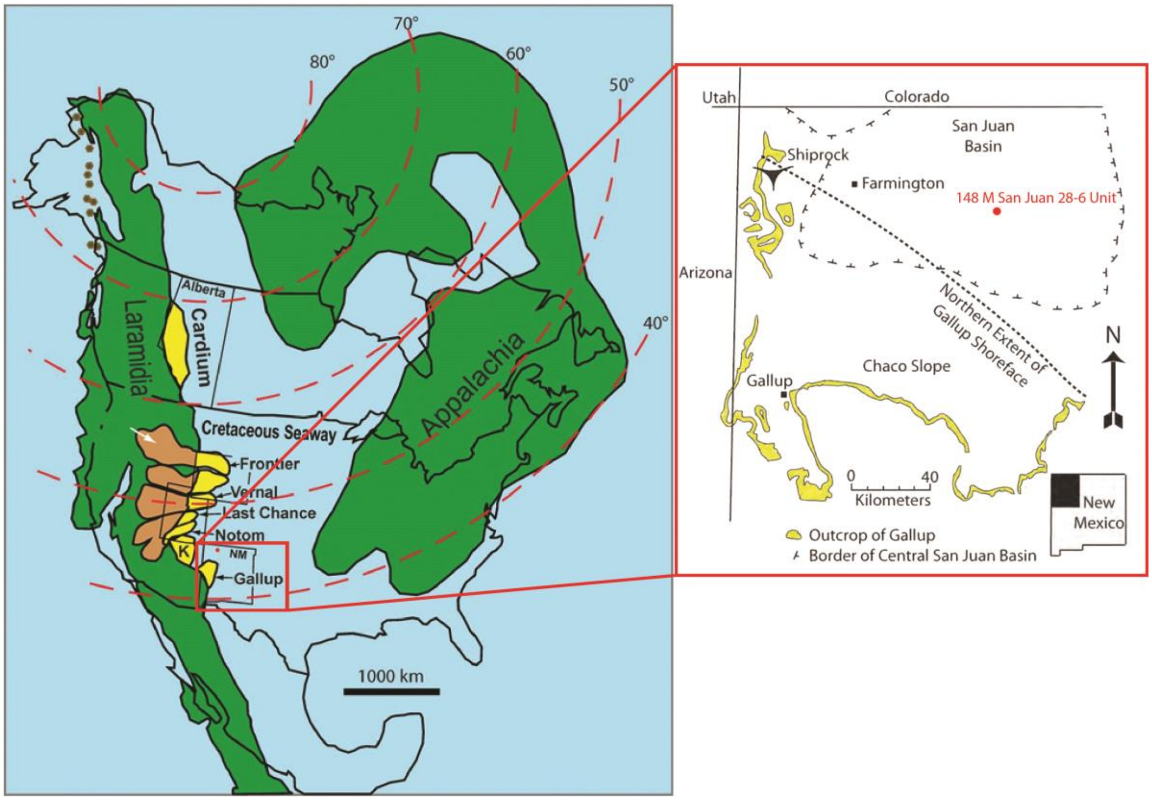

Figure 3: Location of 148 M San Juan 28-6 Unit core in relation to the Cretaceous Western Interior Seaway during the Turonian (modified from Bhattacharya and MacEachern, 2009) and the Gallup outcrop belt (modified from Campbell, 1979).

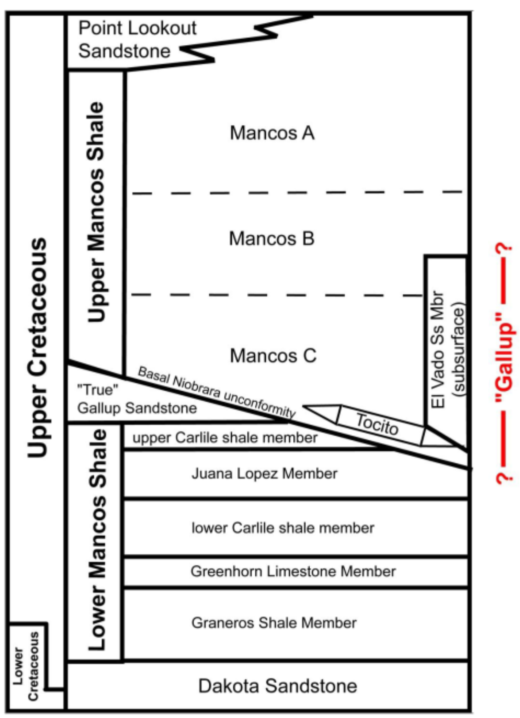

Figure 4: Stratigraphic column of the Mancos Shale, including the division of the Upper Mancos (taken from Broadhead, 2015).

3. Methodology

A detailed thin bedded facies analysis was done on 54 m of slabbed core from the Upper Mancos Shale, Mancos C (figure 5). Thin beds are defined as having thicknesses between 3 and 10 cm (figure 6; Passey et al., 2006). In this study, beds range in thickness from 0.1 mm to 20 cm, but on average the bed thicknesses range from several millimeters to a few centimeters. Sedimentological data, such as grain size, type of sedimentary structures, bed thickness, lithology, clay content, fossils, ichnofacies, and degree of bioturbation were measured for each bed. The tools used to collect the data included a measuring tape, grain size card and hand lens. The core was photographed using a copy stand and SLR camera.

To determine grain size, the Wentworth classification was used. The percentage of clay and silt was determined by chewing the rock and looking at the variations in colour. The lower the clay content, the grittier the rock will feel when chewed, while mudstones with a higher clay content will have a smoother texture. Beds with a low clay content appear lighter and greyish than beds with a high clay content, which usually appear very dark.

The Bioturbation Index was used to determine the degree of bioturbation. A number from zero to six was assigned to distinct units of the core, with 0 representing no bioturbation and six representing complete bioturbation (Taylor and Goldring, 1993). Numerous sections of the core appeared to be structureless and homogeneous mudstone. However, using contrast enhancements as described by Schieber (2003), burrows could be seen in some of these sections.

In order to understand the processes forming the thin beds in the Mancos C, each lamination was measured using detailed photographs of the core. Each lamination had to be measured because the type of sedimentary structures varied almost every millimeter. This detailed analysis proved to be time consuming, as it took almost 3 months to measure all laminations (~10 860) over all 54 m. In addition to this, 2 months were spent in the core lab logging the core and making notes on grain size and clay content. The percentage of each facies was calculated by dividing the total thickness of a facies by the total thickness of a parasequence.

Parasequences (figures 5 and 31) were chosen by looking for sections where grain size increased upwards, as well as looking for sections where the number of laminations increase upwards. Smaller parasequences, i.e., lamina bedsets (figure 31), can also be picked out, however, for this study only the general parasequences were chosen.

Sequence boundaries, lowstand systems tracts, highstand systems tracts, and transgressive sequence tracts were identified. Sequences boundaries were placed where there was a distinct change in facies, for example, where there was a change from a thinly laminated facies to a very thin bedded facies. Lowstand systems tracts were placed above the sequence boundaries, while highstand systems tracts were placed below the sequence boundaries. Transgressive surfaces were placed where *Glossifungites* surfaces were present. Above the transgressive surfaces, fining upward transgressive systems tracts can be found, capped by a maximum flooding surface. The maximum flooding surface is identified by a change in facies from a less laminated muddy facies to a slightly higher laminated facies above the surface.

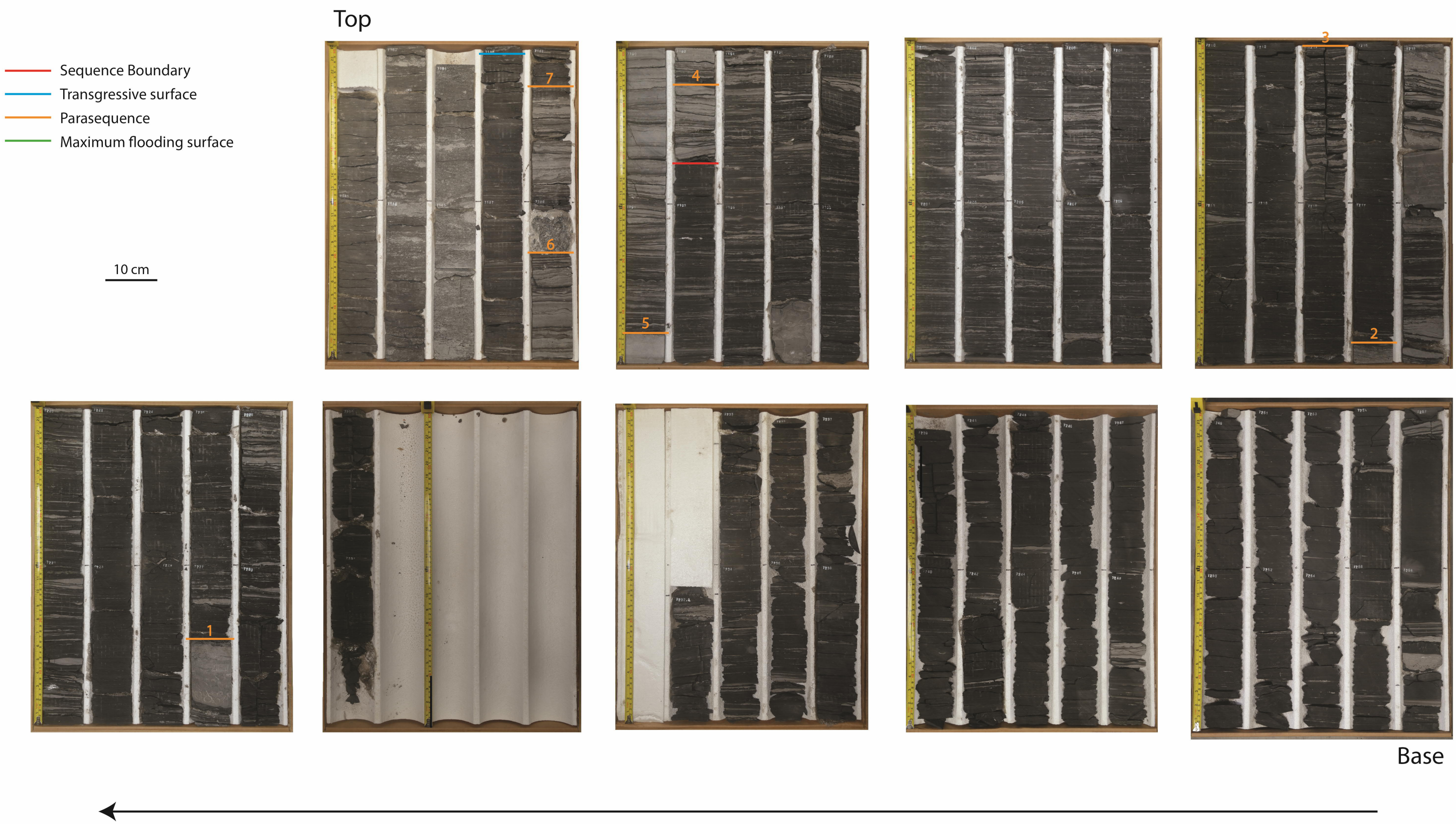

Figure 5: Boxes of Mancos C core analysed. Sequence boundaries, transgressive surfaces, and maximum flooding surfaces are marked. Parasequences are labelled with their number. Black arrow points in the direction of decreasing depth.

Figure 5 continued: Boxes of Mancos C core analysed. Sequence boundaries, transgressive surfaces, and maximum flooding surfaces are marked. Parasequences are labelled with their number. Black arrow points in the direction of decreasing depth.

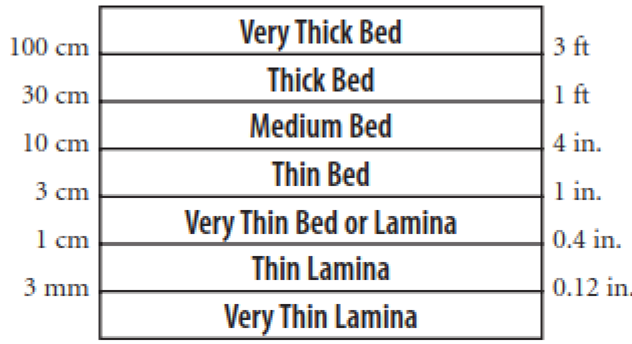

Figure 6: Common terminology for thin beds in the geological literature (taken from Passey et al., 2006)

3.1 Recognition of thin-bedded processes

In deltaic systems, facies can be identified as being generated by fluvial, wave, or tidal dominated processes (Galloway, 1975). However, evidence of mixed processes, where two or three of the fluvial, wave, and tide processes may be expressed, have an influence on these facies (Ainsworth et al., 2011). In the fluvial, wave, and tidal classification, modified by Ainsworth et al. (2011), the area covered by each facies generated by fluvial-, wave-, and tide-dominated processes can be calculated, and the proportion of each depositional process can be determined. The depositional process with the highest proportion dominates deposition, while depositional processes with the moderate and lowest proportions influence and affect deposition respectively (Ainsworth et al., 2011).

Mud is transported offshore by processes such as ignitive turbidites, tempestites, hypopycnal and hyperpycnal flows. Ignitive turbidites are generated from sediment instability or failure, making them short lived events (minutes to days; Normark and Piper, 1991; Mulder et al., 2003; Pattison, 2005). Their deposits typically show the T_A, T_B, T_C, T_D, and T_E divisions of the Bouma sequence (figure 7; Bouma, 1962). The T_E division can be further divided to describe fine-grained turbidites (Piper, 1978; Li et al., 2015). Hyperpycnites, produced by hyperpycnal flows, are characterized by an inversely graded basal unit overlain by a normally graded Bouma sequence (Mulder et al., 2003). Depending on the relative duration and strength of waxing vs. waning flow, these inverse and normally graded units may be marked by a scour. Hypopycnal flow deposits are identified by moderately to highly bioturbated units. Wavy laminations and storm wave ripples are characteristic of tempestites. Waves and tides can aid to these processes allowing the formation of fluid muds, which can travel down slopes as shallow as 0.03^{o} (Schieber, 2016). Fluid muds typically form homogenous and structureless mudstone layers with a thickness of 0.5 to >~1 cm, and lack bioturbation, grading and internal laminations (Dalrymple et al., 2003). Finally, typical tidal deposits include mud drapes, tidal rhythmites, and flaser, wavy, and lenticular bedding.

Ignitive turbidites, hypopycnal and hyperpycnal flows are river fed, indicating a fluvial influence, while tempestites indicate a wave/storm influence.

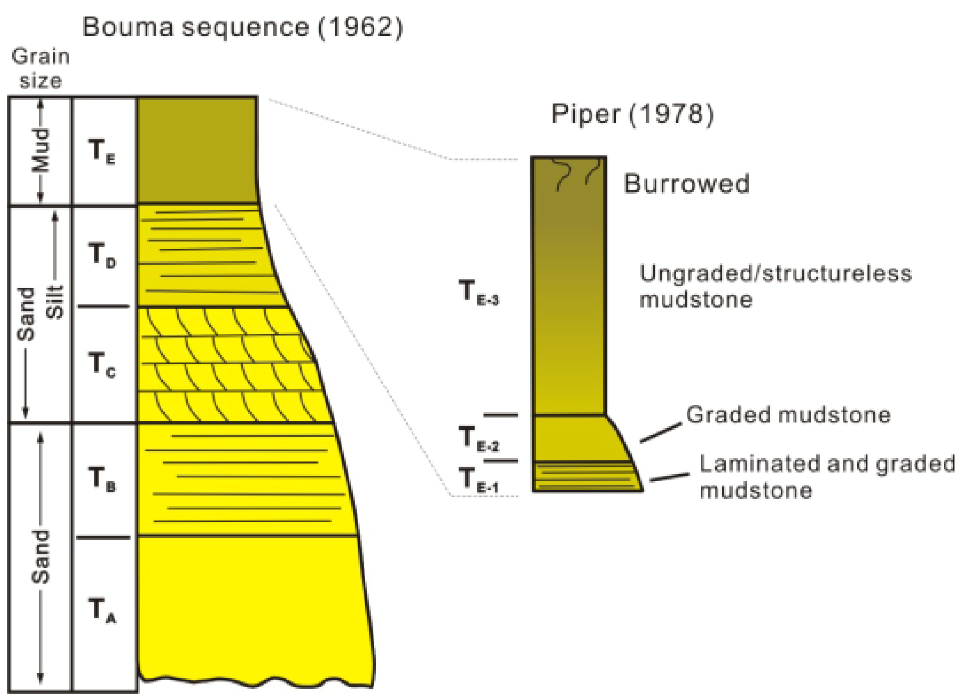

Figure 7: Bouma Sequence exhibiting a fining upward succession. Divisions TA, TB, TC, TD, and TE are displayed. A division of TE, proposed by Piper (1978), is also displayed (taken from Li et al., 2015).

4. Facies Description and Interpretation

A total of 12 facies were observed within the Mancos C core. Twenty parasequences, showing coarsening upward facies, were picked (figure 5). *Inoceramid* fragments were present throughout the entire Mancos C section. The 12 facies are described and interpretated below, and a facies key is shown in figure 8.

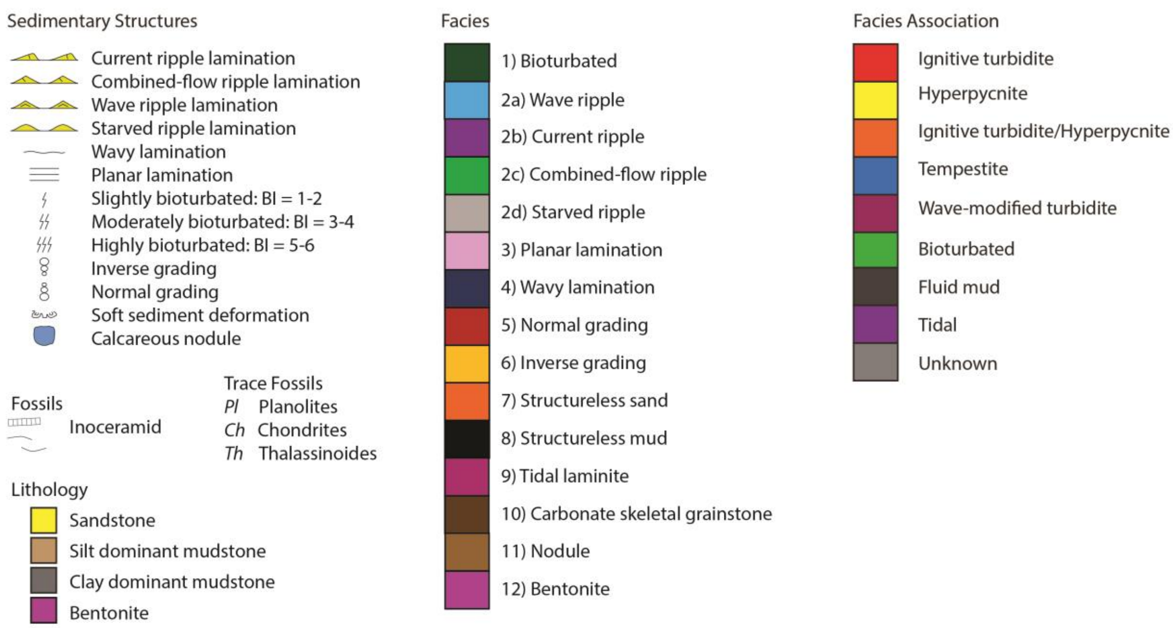

Figure 8: Facies key for stratigraphic sections

Facies 1: Bioturbated

Some mudstone units show moderately to highly bioturbated facies (BI = 3-6; figure 9). Some of these burrows could not be named, but identifiable burrows such as *Planolites*, *Zoophycos*, *Chondrites*, *Thalassinoides*, and *Phycosiphon* could be identified throughout other sections of the core (figure 10). This facies ranges in thickness from 1 mm (very thin lamina) to 6.7 cm (thin bed). The highest proportion of this facies occurs in parasequence 20 at 15.8%, while the lowest proportion can be found in parasequence 4 at 0.53%.

Also included in this facies is a highly bioturbated fine upper grained glauconitic muddy sandstone (figures 11 and 12). In this facies the trace fossils recognized are *Planolites* and *Thalassinoides*.

Interpretation

In this study, the highly bioturbated mudstone facies is interpreted to represent low sedimentation rates (MacEachern et al., 2005). The majority of these trace fossils belong to the distal *Cruziana*- proximal *Zoophycos* ichnofacies, having a depth >50 m and <100 m, therefore they indicate deposition in a fully marine setting, well below fair-weather wave base (MacEachern et al., 2005). The abundance of wave ripple laminations indicates deposition above storm wave base.

In hypopycnal flows, river water containing fine-grained sediments, such as clay and silt, tends to float on denser marine water as a buoyant plume (Bates, 1953). These buoyant plumes can extend offshore for tens of kilometers, where the suspended sediment flocculates and settles out onto the basin floor (Nemec, 1995; Schieber, 2016). It is possible that the mud settled slowly enough to allow enough time for the sediment to be reworked by organisms. As mentioned above, this facies was deposited in a marine setting therefore this facies can be classified as a marine event bed. It is also important to note that hypopycnal plumes can be deflected alongshore, for 1000s of kilometers, by Coriolis forces (Kineke et al., 1996; Nittrouer et al., 1996; Correggiari et al., 2005)

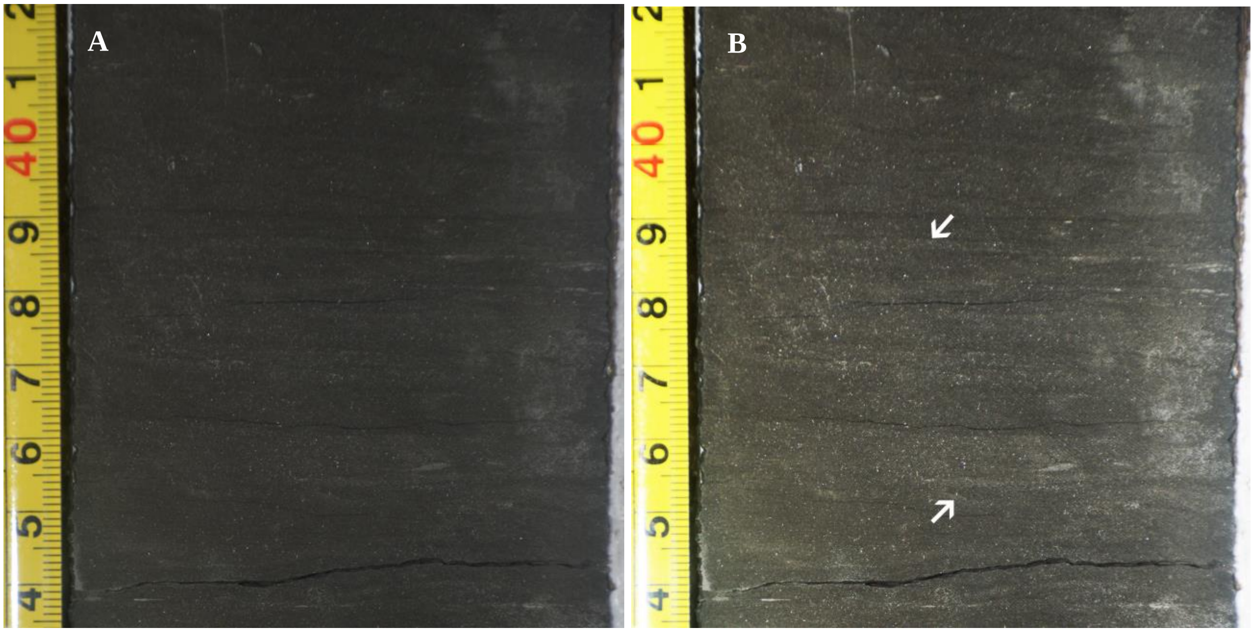

Figure 9: Black shale showing cryptobioturbation located at 7258 ft. (A) Original image. (B) Contrast has been increased to help distinguish the burrows. Arrows are pointing to burrows. Scale is in centimeters.

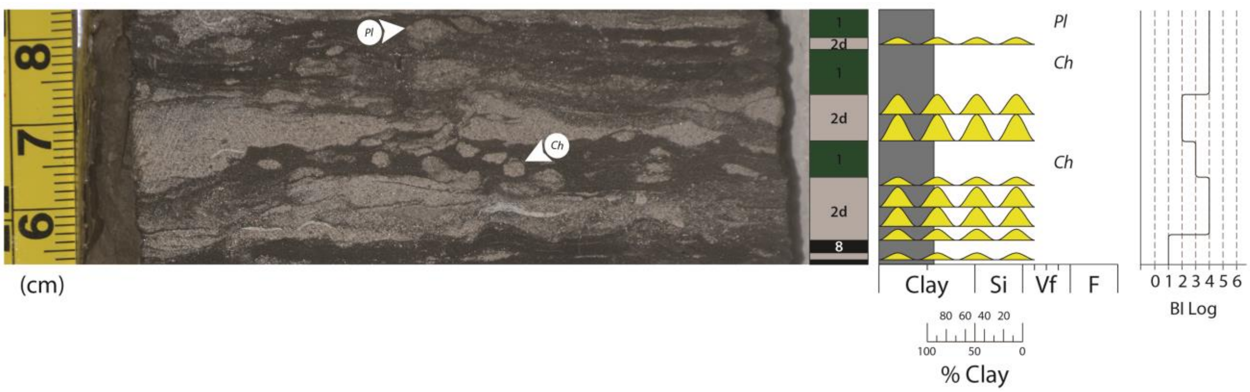

Figure 10: Bioturbated units showing *Chondrites* (Ch) and *Planolites* (Pl) at a depth of 7228 ft. Correlated facies, measured section, and BI log are also included. See figure 8 for facies key.

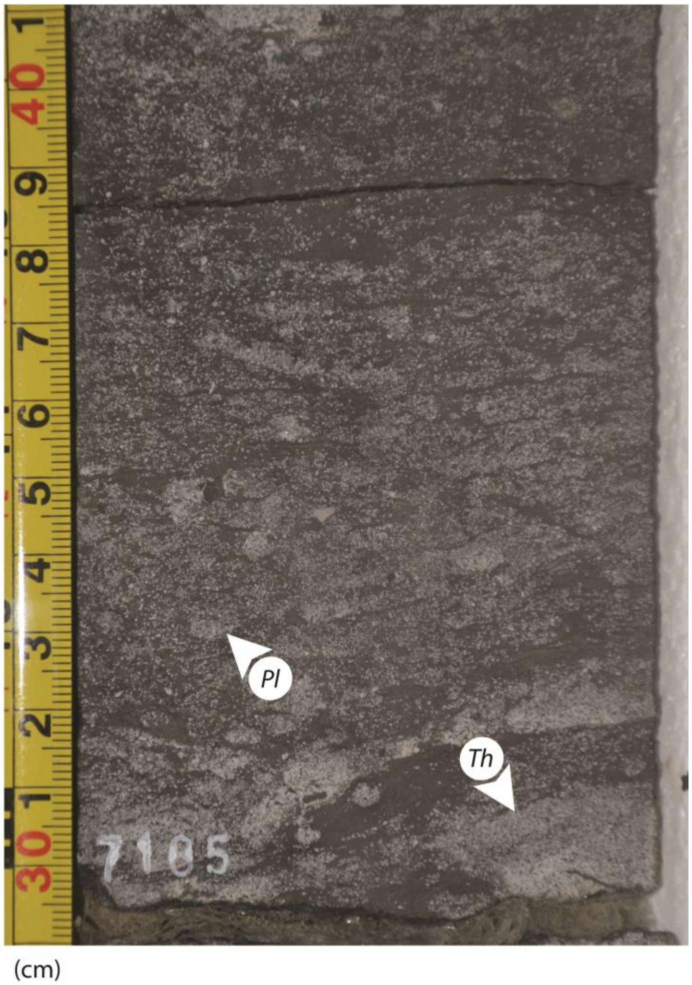

Figure 11: Highly bioturbated (BI = 5-6) glauconitic muddy sandstone, located at a depth of 7184.7 ft.

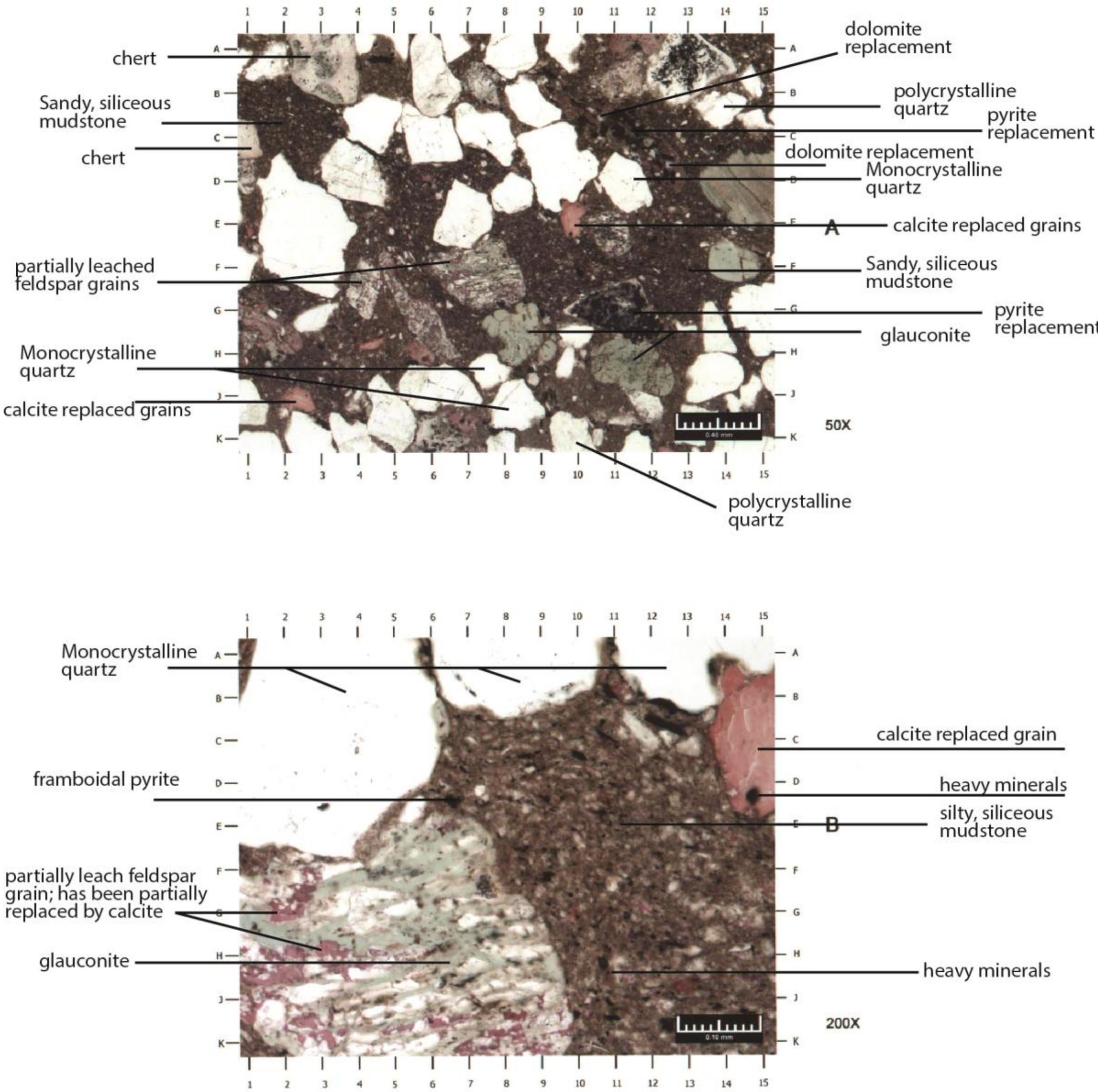

Figure 12: Thin sections of bioturbated glauconitic muddy sandstone, located at a depth of 7184.7 ft., obtained from Weatherford Laboratories (2010).

Facies 2: Rippled laminations

Facies 2a: Wave ripple laminations

Wave rippled laminations consist of very fine lower to fine lower sand and show evidence of oscillatory flow (figure 13). Wave ripples were identified by their symmetrical, rounded crests, and internal laminae dipping in two directions showing a concave downward shape (figure 14). The wave ripples are present as both starved ripples and continuous rippled laminations, and some have an erosive base. The thickness of this facies ranges from 0.1 mm (very thin lamina) to 2 cm (very thin bed). The highest proportion of this facies is found in parasequence 6 at 21.1%. The lowest proportion is found in parasequence 14 at 0.35%. Bioturbation within these units is low, with a BI ranging from 0 to 3.

Interpretation

In deeper water environments, wave ripples form as the result of oscillatory motion, likely from storm generated waves (Myrow et al., 2002), rather than fair-weather waves. The presence of starved wave ripples in these parasequences is evidence of strong flow from large storms, with limited sediment supply (Lock et al., 2009). Therefore, this facies is interpreted to be deposited by tempestites, and is classified as storm wave-dominated.

Tempestites are normally graded and therefore associated with waning flow. They are identified by an erosional surface, cut by a storm event, that is overlain by low-angle laminated to hummocky cross-stratified sands (Suter, 2006). As the storm weakens, wave ripples and/or combined-flow ripples form (Suter, 2006). Once the storm ends, a mud drape, produced from suspension fallout, caps the sequence (Suter, 2006). Storm waves are capable of resuspending sediment to produce wave-enhanced sediment gravity flows (WESGFs; Macquaker et al., 2010). WESGFs are preserved as a triplet bed which consists of an erosional surface overlain by sand ripple laminae, followed by a wavy parallel lamina set composed of alternating silt and clay laminae, with the entire sequence being capped by a structureless mud (Macquaker et al., 2010). This tripartite division of sand-silt-mud was rarely observed within the Mancos C core.

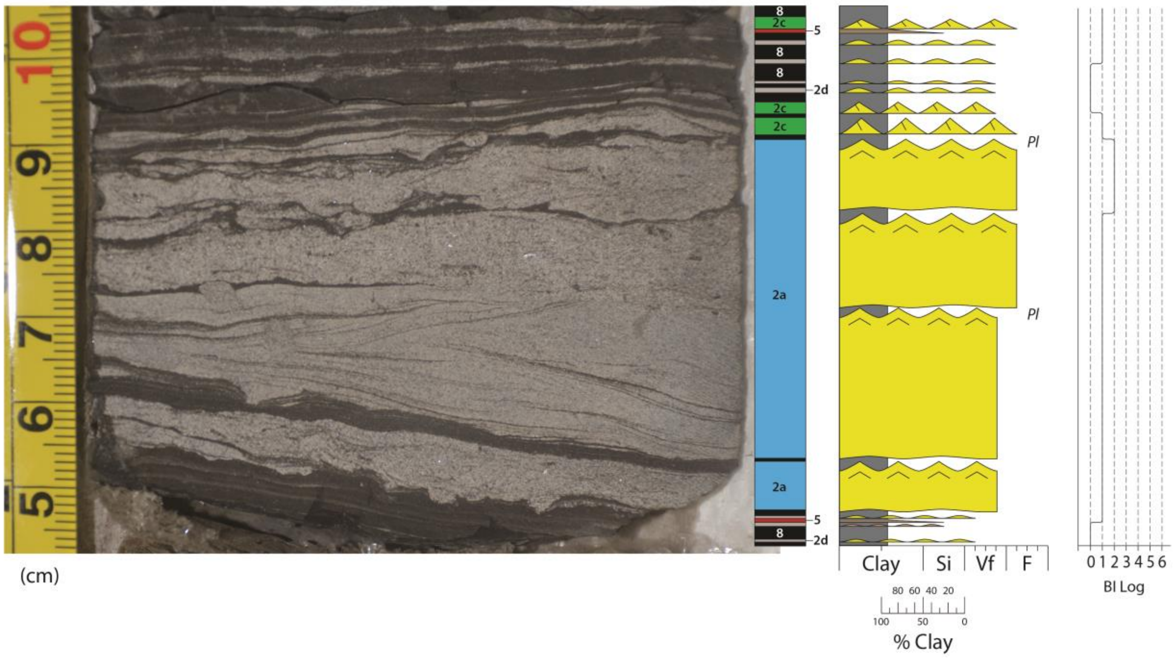

Figure 13: Very fine upper to fine lower sandstones with wave ripple laminations, located at a depth of 7219.8 ft., with correlated facies, measured section, and BI log. See figure 8 for facies key.

Figure 14: Wave rippled sandstones at a depth of 7219.8 ft. Line drawing highlights cross laminations dipping in two directions. Some of these laminations have a concave down shape and have a mounded appearance.

Facies 2b: Current ripple laminations

Current ripple laminations consist of very fine lower to fine lower sand and show evidence of unidirectional flow (figure 15). The unidirectional component of flow is evident from foresets dipping in one direction, downlapping the basal surface (figure 16). The crests of current ripples are usually asymmetric, however some current ripples in the core show a relatively flat top. This facies is seen as both starved and continuous rippled laminations, and some of these ripples have an erosive base. The thickness of this facies ranges from 0.3 mm (very thin lamina) to 0.4 cm (thin lamina). Its highest proportion, of 4.9%, is found in parasequence 6, while its lowest proportion, of 0.04%, is found in parasequence 15, and in general, current ripples are minor compared to wave-formed sedimentary structures. These units either show no signs of bioturbation or are lightly bioturbated, with a BI ranging from 1 to 2.

Interpretation

Current ripples are the result of unidirectional flow which produces ripples with a gently sloping stoss side and a steep lee side (Reineck and Singh, 1973). Current ripples are common in the T_C division of the Bouma sequence (figure 15; Bouma, 1962). This facies is attributed to river fed hyperpycnal flows and ignitive turbidity currents and thus this facies represents fluvial dominant processes.

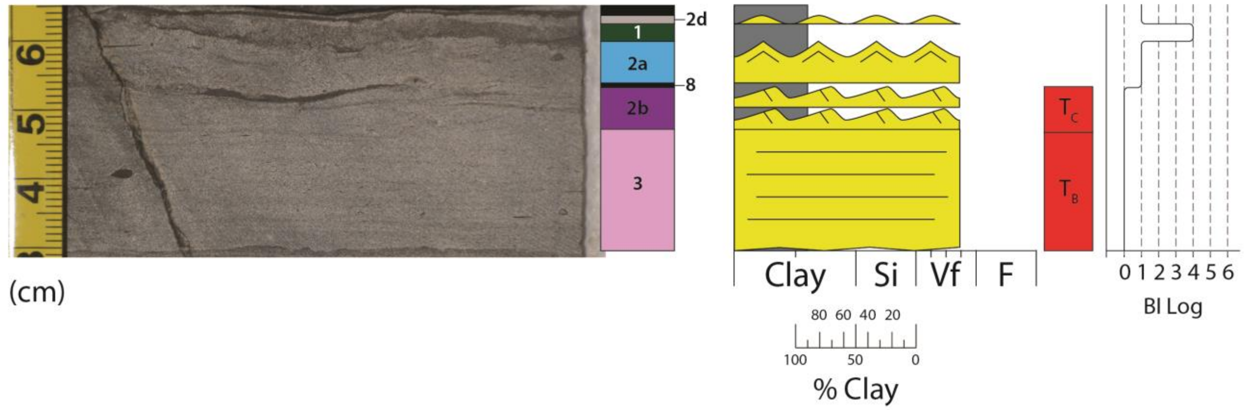

Figure 15: Very fine upper sandstones with planar laminations, current ripples, and wave ripples, located at a depth of 7190.5 ft., with correlated facies, measured section, and BI log. T_B and T_C divisions of the Bouma sequence are also labelled. See figure 8 for facies key.

Figure 16: Parallel laminate to current ripple sandstone at a depth of 7190.5 ft. Line drawing highlights dipping foresets.

Facies 2c: Combined-flow ripple laminations

Combined-flow ripple laminations consist of very fine lower to very fine upper sand and show evidence of both unidirectional and oscillatory flows (figure 17). The unidirectional component is evident from high angle foresets (< 25°) dipping in one direction, downlapping the basal surface (figure 18). The oscillatory motion overprints the unidirectional component, and is evident from the symmetrical crest of the combined-flow ripple. This facies is seen as both starved and continuous rippled laminations, and some of these ripples have an erosive base. The thicknesses of this facies range from 0.5 mm (very thin lamina) to 0.8 cm (thin lamina). The highest proportion of this facies is found in parasequence 6 at 5.13%, and its lowest proportion is found in parasequence 14 at 0.03%. Again, this facies is minor and about equivalent in percentage to current ripples. The BI of this facies ranges from 0 to 2.

Interpretation

Combined-flow ripples present in these parasequences show dipping foresets overprinted by oscillatory wave motion, which indicates both fluvial and wave influence. Combined-flow ripples are likely the result of storm-induced tempestites, which include both oscillatory and density-induced flows (Myrow et al., 2002), or wave-modified turbidites. Therefore, this facies can be classified as both fluvial and storm wave-dominated.

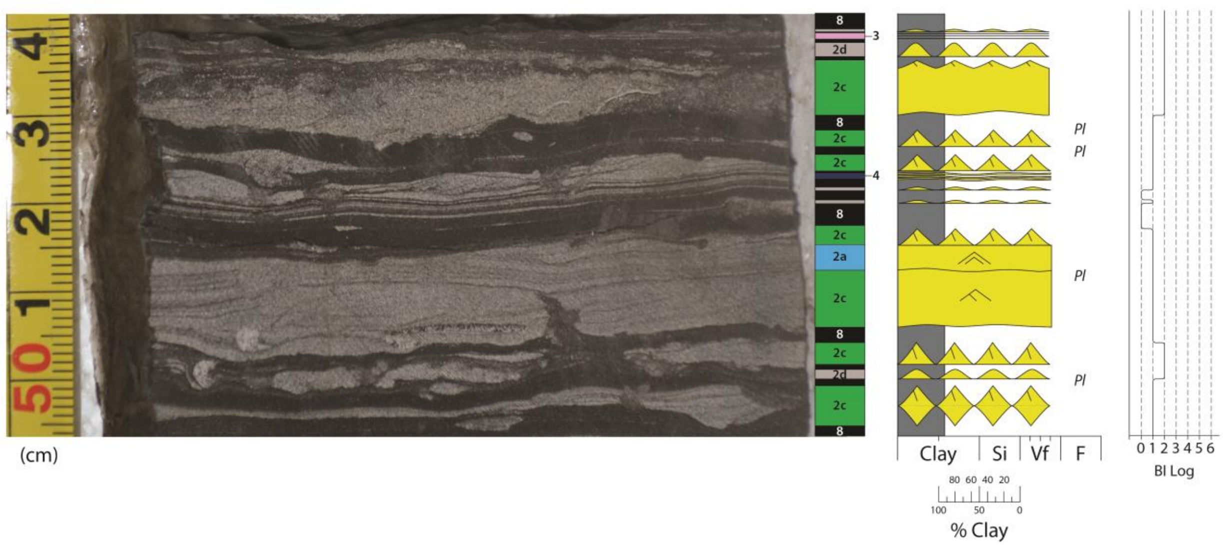

Figure 17: Multiple very fine upper combined-flow ripples and wavy laminations, located at a depth of 7228.4 ft., with correlated facies, measured section, and BI log. See figure 8 for facies key.

Figure 18: Combined-flow ripples at a depth of 7219.8 ft. Line drawing highlights foresets dipping to the right of the core, indicating unidirectional flow. Overprinted on these foresets is a symmetrical mounded crest indicating oscillatory wave motion.

Facies 2d: Starved ripple laminations

Starved ripples consist of silt to fine lower sand lenticular beds with no clear evidence of unidirectional or symmetrical cross laminations (figure 19). The thickness of this facies ranges from 0.1 mm to 1.1 cm. This facies has a BI index ranging from 0 to 2, meaning that units either show no bioturbation or are lightly bioturbated. This facies occurs in all parasequences with its highest proportion of 24.7% located in parasequence 5, and its lowest proportion of 3.1% located in parasequence 19.

Interpretation

These starved ripples were produced by either unidirectional or symmetrical ripple processes. However, because lamina symmetry could not be established, it was not possible to confidently conclude what process produced the starved ripples. With magnified photo enhancement and thin section analysis it would be possible to see if there are any cross laminations. It is likely they these ripples are the result of storm waves, since wave ripples (facies 2a) make up a greater percentage than current and combined-flow ripples.

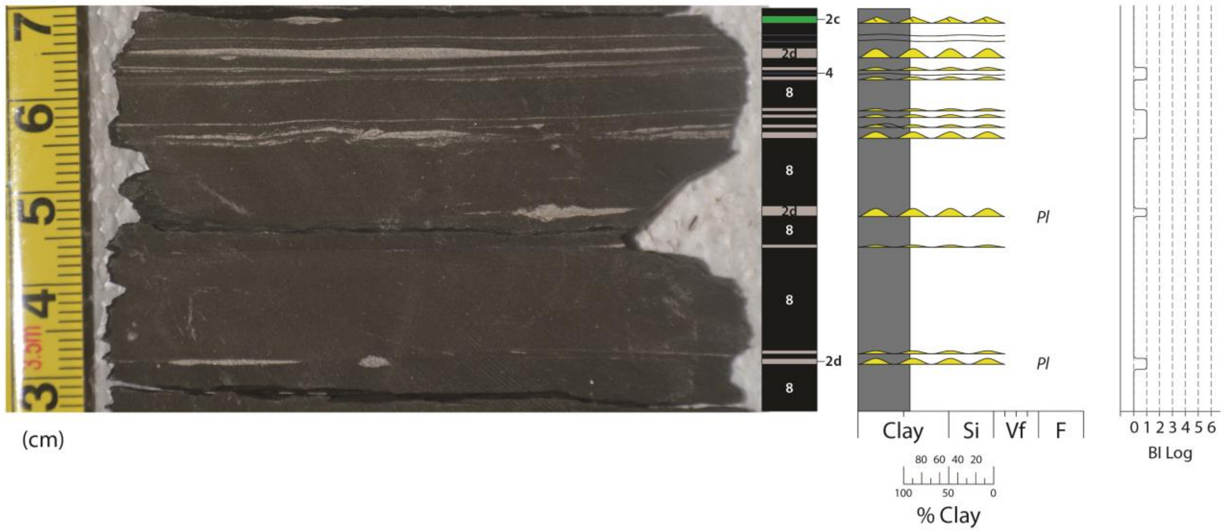

Figure 19: Starved ripples where cross-laminations could not be observed, located at a depth of 7256.8 ft., with correlated facies, measured section, and BI log. See figure 8 for facies key.

Facies 3: Planar laminations

Planar laminations found in this study are composed of silt to very fine upper sand (figure 20). The thicknesses of these unit range from 0.1 mm (very thin lamina) to 1.7 cm (very thin bed). The highest proportion of this facies occurs in parasequence 11 at 3.55%, while the lowest proportion occurs in parasequence 10 at 0.18%. These laminations show little to no bioturbation, with a BI ranging from 0 to 2. Some planar laminations have a rhythmic appearance (figure 20), indicating a possible tidal influence.

Interpretation

Planar laminations commonly indicate continuous sediment deposition by suspension settling (Lazar et al., 2015). Processes such as hypopycnal flows, hyperpycnal flows, and ignitive turbidites are capable of depositing planar laminations, therefore this facies has been classified as fluvial-dominated. These planar laminations have a low BI index which implies a moderate to high sedimentation rate (MacEachern et al., 2005).

Figure 20: Silty parallel laminations, at a depth of 7238.1 ft., with correlated facies, measured section, and BI log. See figure 8 for facies key. Part of the photo was shifted down to display its original view. Laminations look rhythmic, indicating a tidal influence.

Facies 4: Wavy laminations

Wavy laminations in this study are composed of silt to very fine upper sand (figure 21). Thicknesses of these units range from 0.1 mm (very thin lamina) to 1.3 cm (very thin bed). Parasequence 6 has the highest proportion of this facies at 6.53%, while parasequence 10 has the lowest at 0.05%. These units are either lightly bioturbated (BI = 1-2) or show no evidence of bioturbation.

Interpretation

Wavy laminations are likely to have been deposited by oscillatory flow from tempestites. Therefore, this facies is classified as storm wave-dominated. The low BI index of this facies again implies a moderate to high sedimentation rate (MacEachern et al., 2005).

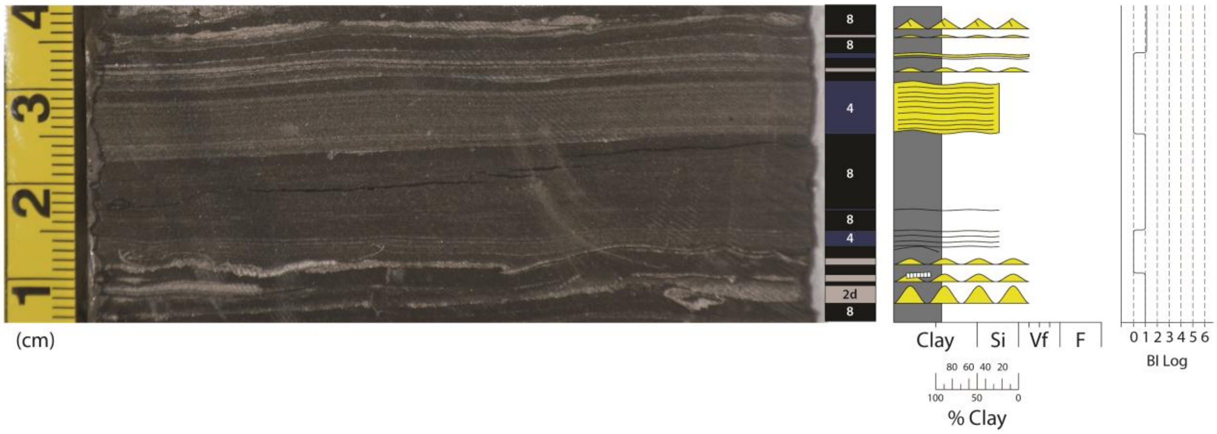

Figure 21: Millimeter scale very fine lower wavy laminations, located at 7195.6 ft., with correlated facies, measured section, and BI log. See figure 8 for facies key.

Facies 5: Normal grading

Normally graded beds, where grain size decreases upward from very fine lower sand to clay are present in a couple of parasequences (figure 22). These units range in thickness from 0.1 mm (very thin lamina) to 1.4 cm (very thin bed), and some have an erosive base. The highest proportion of this facies occurs in parasequence 4 at 3.1%, and the lowest proportion occurs in parasequence 14 at 0.01%. Bioturbation within these beds is low, BI = 0-1.

Interpretation

Normal grading is the result of a decreasing or waning flow (Mulder et al., 2003). As a flow decreases in velocity, it will initially deposit coarser sediments followed by the deposition of finer and finer sediments as the flow velocity continues to drop (Mulder et al., 2001). In this study, when a normally graded unit is followed by an inversely graded unit, it can be attributed to hyperpycnal flows. If the unit is only normally graded, then it can be attributed to ignitive turbidites, tempestites, or suspension settling. A majority of the normally graded units are either massive or planar laminated, and therefore can be associated with river fed ignitive turbidites, hyperpycnal or hypopycnal flows.

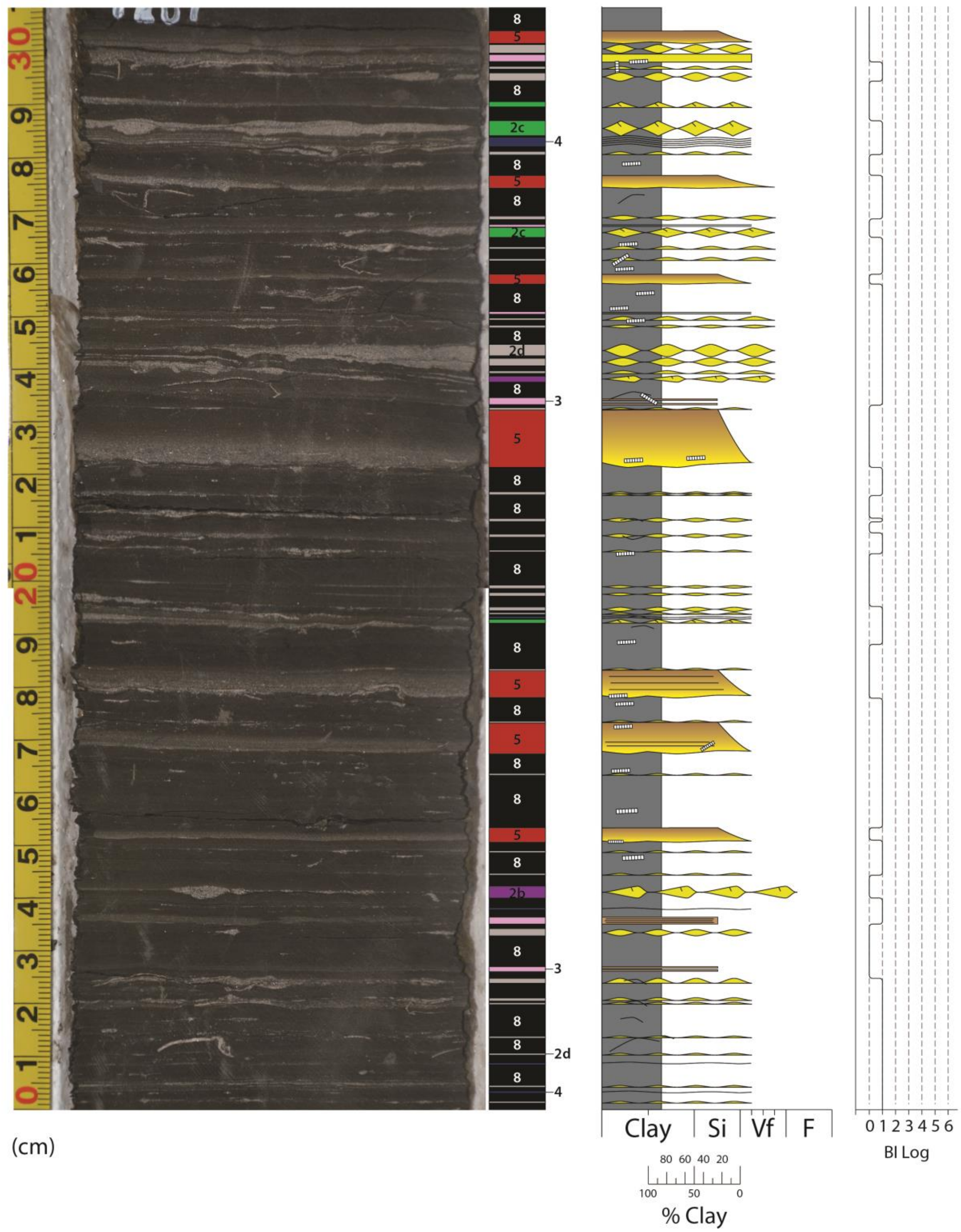

Figure 22: Seven normally graded units decreasing in grain size from very fine lower sand to mud, located at a depth of 7207 ft. Correlated facies, measured section, and BI log are also included. See figure 8 for facies key.

Facies 6: Inverse grading

Some parasequences have inversely graded beds, where grain size increases upward from clay to very fine lower sand (figure 23). These units range in thickness from 0.4 mm (very thin lamina) to 0.45 cm (thin lamina), and some have an erosive base. This facies is present in exceedingly small amounts, with its lowest proportion of 0.02% located in parasequence 14, and its highest proportion of 0.6% located in parasequence 6. The inversely graded beds show no signs of bioturbation within the bed.

Interpretation

Inverse grading is the result of an increasing or waxing flow (Mulder et al., 2003). As a flow increases in velocity, finer sediments will be deposited first followed by the deposition of coarser sediments (Mulder et al., 2003). Inverse grading is thought to be diagnostic of hyperpycnal flows. Hyperpycnal flows form when the density of river water is greater than that of the marine environment which it is entering (Mulder et al., 2003). Areas with steep slopes (> 0.7^{o}) are required to carry mud far offshore (Milliman and Syvitski, 1992; Bentley, 2003; Schieber, 2016).

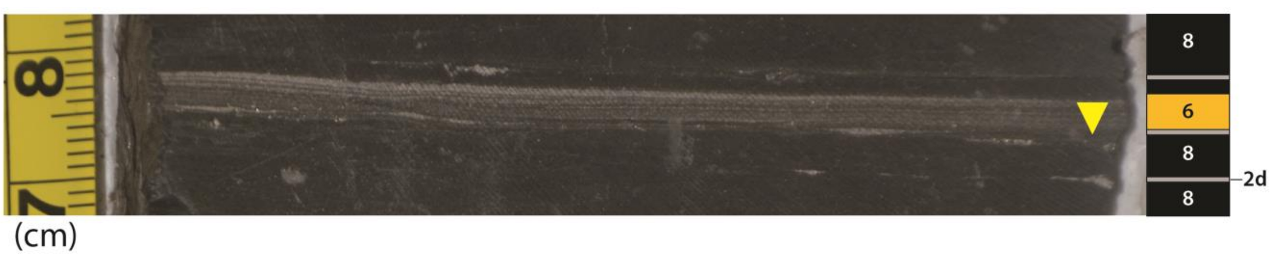

Figure 23: Inversely graded lamina set located at 7209.4 ft, with correlated facies. Grain size increases from silt to very fine lower sand. See figure 8 for facies key.

Facies 7: Structureless sandstone

Structureless sandstone, consisting of very fine lower to fine upper sand, is present within a few paraseqeunces (figure 24). The thickness of these units range from 0.3 cm (thin lamina) to

2.1 cm (very thin bed). The highest proportion of this facies is found in parasequence 5 at 45%, while its lowest proportion is found in parasequence 1 at 0.53%. This facies appears homogeneous and lacks any internal sedimentary structures, however some units show signs of soft sediment deformation.

Interpretation

The lack of internal structures suggests that sand was deposited very rapidly from suspension or from very highly concentrated sediment dispersions during sediment-gravity flows (Lowe, 1982; Kneller and Branney, 1995; Talling et al., 2012). In the case of this study, this facies can be a result of hyperpycnal flows, ignitive turbidites, or slurry/debris flows, and is classified as fluvial-dominated.

Figure 24: Structureless sandstone bed at a depth of 7191.8 ft., with correlated facies. See figure 8 for facies key.

Facies 8: Structureless mudstone

Structureless mudstone consists of grain sizes ranging from clay to silt, and lacks any internal sedimentary structures (figure 25). Bioturbation is low, with a BI ranging from 0 to 2. This facies has thicknesses ranging from 0.2 mm (very thin lamina) to 17.2 cm (medium bed). The highest proportion of this facies can be found in parasequence 19 at 93.1%, while the lowest proportion can be found in parasequence 5 at 15.3%.

Interpretation

Because the majority of the Mancos C core is composed of structureless mudstone it is likely that these layers are fluid muds. Fluid muds are bottom-hugging mobile bodies of fine-grained sediment, clay and silt, with a concentration of solids >10 g L^{-1} (Kirby and Parker, 1983). Mud originally deposited in shallow water was likely resuspended by wave action forming a fluid mud that is able to move downslope across the shelf under the influence of gravity (Traykovski et al., 2000; Friedrichs and Wright, 2004). These fluid mud units either lack bioturbation or are lightly bioturbated (BI = 1-2), indicating that the muds accumulated relatively quickly within hours (Ichaso and Dalrymple, 2009). The rarity of tidal facies within the Mancos C in this core suggests that tides did not play a major role in forming fluid muds. Therefore, this facies can be classified as storm wave-dominated.

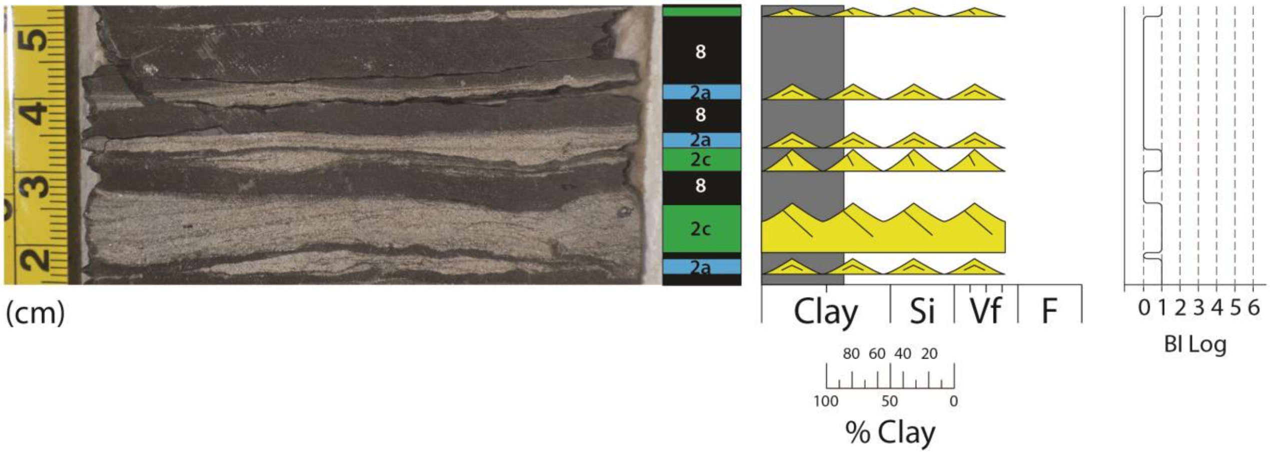

Figure 25: Massive mudstone units in between combined-flow and wave ripples. Located a depth of 7219.6 ft. Correlated facies, measured section, and BI log are also included. See figure 8 for facies key.

Facies 9: Tidal laminite

Tidal laminites consist of clay and very fine lower sand, and range in thickness from 1 to 2 cm (very thin bed) (figure 26). Only three parasequences display this facies and the relative proportions are as follows: parasequence 3 at 0.84%, parasequence 4 at 0.29%, and parasequence 8 at 0.54%. This facies looks to have a rhythmic pattern with alternating mud and sand laminations. The BI of these units range from no bioturbation to a BI of 1.

Interpretation

Tides are periodic fluctuations in water level caused by the gravitational attraction of the moon and sun deforming the ocean surface (Dalrymple, 2010). The positions of the moon and sun relative to earth produce varying tidal ranges (Dalrymple, 2010). When the sun, moon, and Earth are nearly aligned, greater than average tidal ranges, called spring tides, occur (Kvale, 2006). Tidal ranges that are smaller than average, called neap tides, occur when the sun and moon are at right angles to the Earth (Kvale, 2006). The neap-spring variation for semi-diurnal tides has a period of 14.77 days and contains 28 tidal cycles (Kvale, 2006; Dalrymple, 2010).

Tidal laminites show a rhythmic pattern of alternating sand and mud that typically represent a single tidal cycle (Dalrymple, 2010). Planar laminations associated with tidal laminites are deposited from suspension, with sand being deposited during the middle of each ebb and flow tide, when current speeds are at their greatest (Nio and Yang, 1991; Dalrymple, 2010). Changes in tidal ranges are seen within the rock record as changes in layer thickness (Nio and Yang, 1991). Spring tides typically deposit thicker layers than neap tides (Dalrymple, 2010). Deposits that do not show rhythmic cyclicity are termed non-cyclic rhythmites (Dalrymple, 2010).

Tidal bundle thickness plots were not conducted for this study, so it is unknown whether these deposits were produced by tides. However, the rhythmic look to the deposits suggests that there is a possibility that they are tidal, so they were included in this study.

Work on the Mancos A of this core by Dosen (2017) focused more directly on tidal deposits (figure 27). Dosen (2017) created tidal bundle thickness plots (figure 28) to determine if these deposits are tidal. It was concluded that these deposits are non-cyclic rhythmites since they do not show 28 tidal cycles between neap-spring tides (Dosen, 2017). This indicates that tides were a process that transported sediment within the Mancos Shale, however, other processes such as waves likely interfered with tidal deposition (Dosen, 2017).

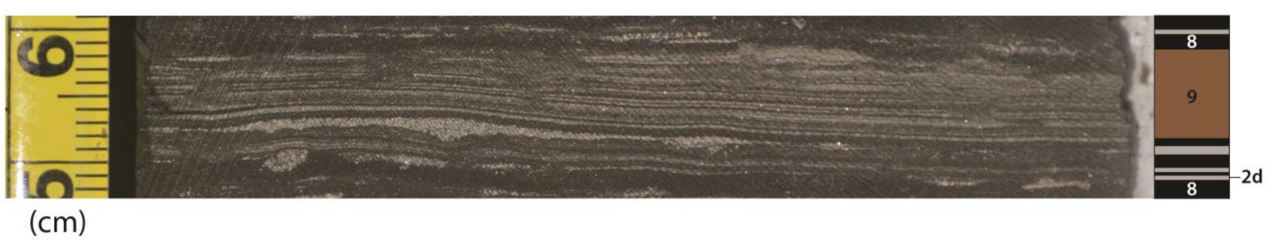

Figure 26: Tidal laminate with alternating laminations of very fine sand and mud, displaying a rhythmic pattern. Located at a depth of 7213 ft. Correlated facies are also included. See figure 8 for facies key.

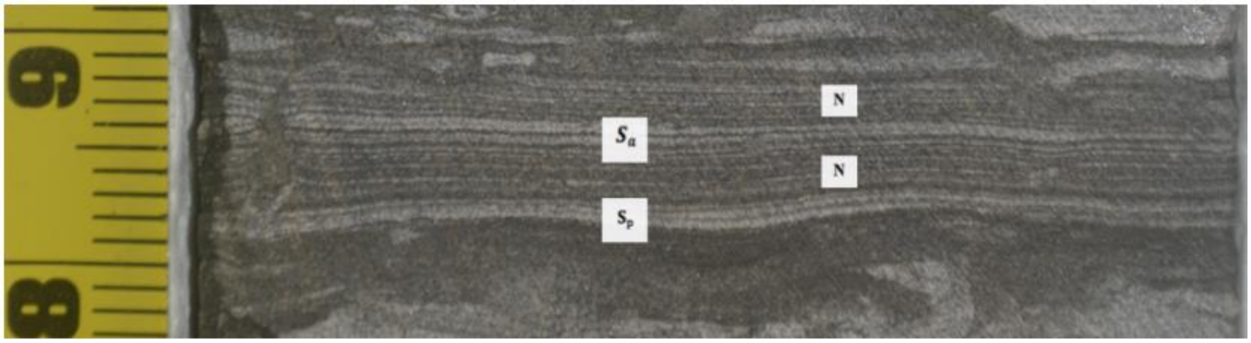

Figure 27: Rhythmically laminated sample within the Mancos A of the 148 M San Juan 28-6 Unit core, located at a depth of 6104.6 ft. Spring perigee (***S$_p$***), sping apogee (***S$_a$***), and neap (N) deposits are labelled (taken from Dosen, 2017).

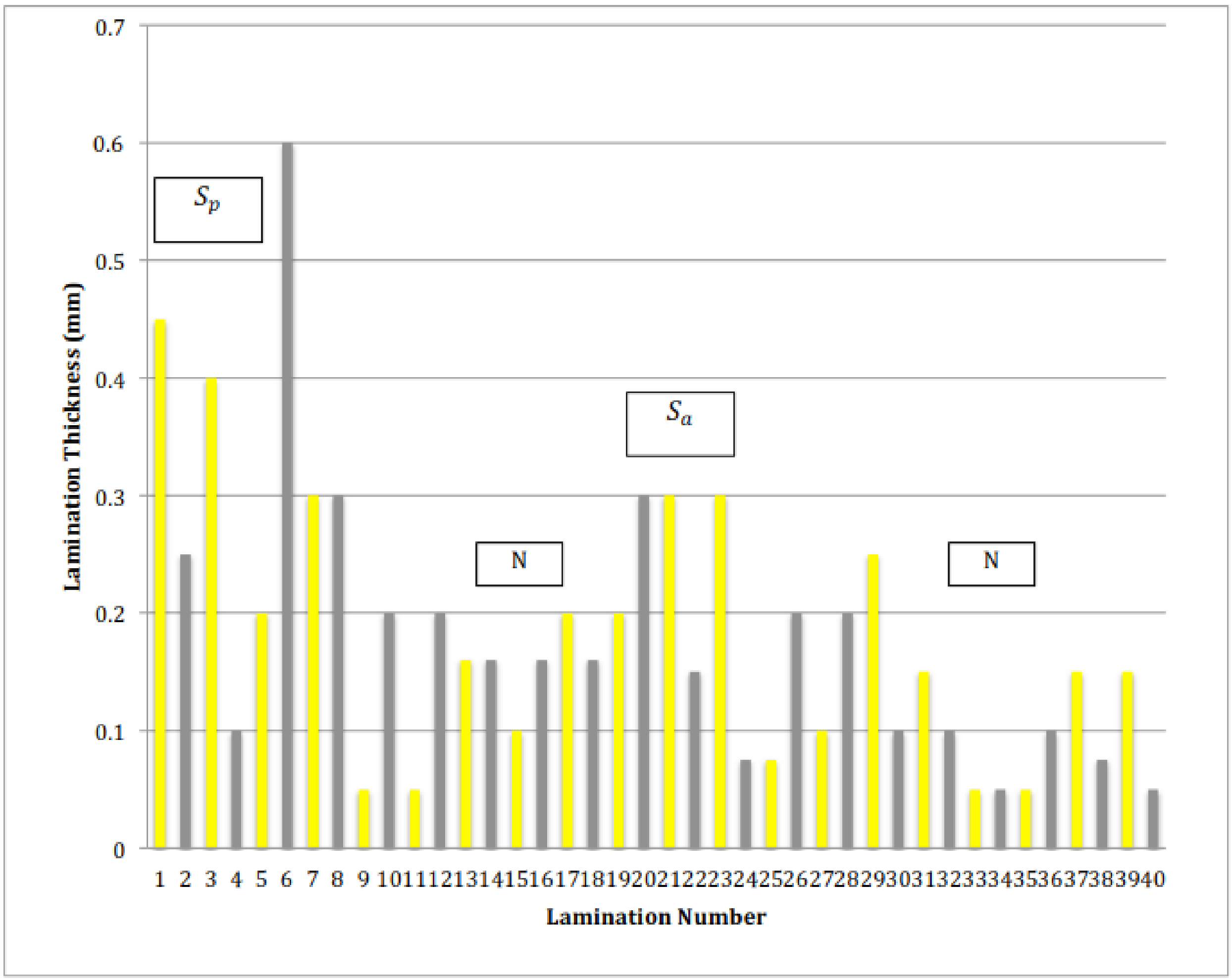

Figure 28: Lamination thickness (mm) plotted against lamination number for the rhythmically laminated sample in figure. Yellow bars represent sand laminations and grey bars represent clay laminations. Possible spring-neap variations in tidal cyclicity, and perigee and apogee are labelled (taken from Dosen, 2017).

Facies 10: Carbonate Skeletal Grainstone

Carbonate skeletal grainstone layers consist of very fine lower to very fine upper sand sized carbonate fragments (figure 26). The thicknesses of these units range from 0.7 cm to 3 cm, and are found in parasequence 17 at a proportion of 1.98% and in parasequence 18 at 1.19%. These units consist primarily of *Inoceramus* fragments, bivalve fragments, foraminifer tests, and phosphatic (fish) particles (figure 27).

Interpretation

Some of the grainstone layers show cross laminations dipping in two directions indicating wave action (figure 28). Tempestite deposits with wave ripples have been observed in carbonates (e.g., Aigner, 1982). Therefore, the grainstone layers within this core can be classified as storm wave-dominated.

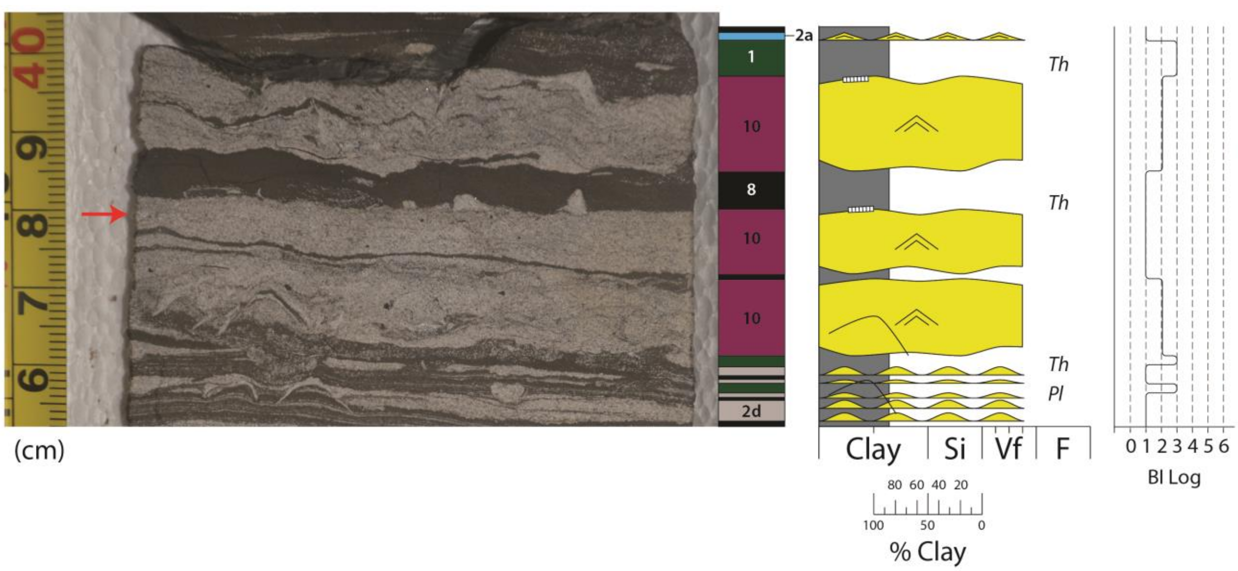

Figure 26: Carbonate skeletal grainstone layers, at a depth of 6920.8 ft, with correlated facies, measured section, and BI log are also included. See figure 8 for facies key. Red arrow indicates location of thin sections in figure 27.

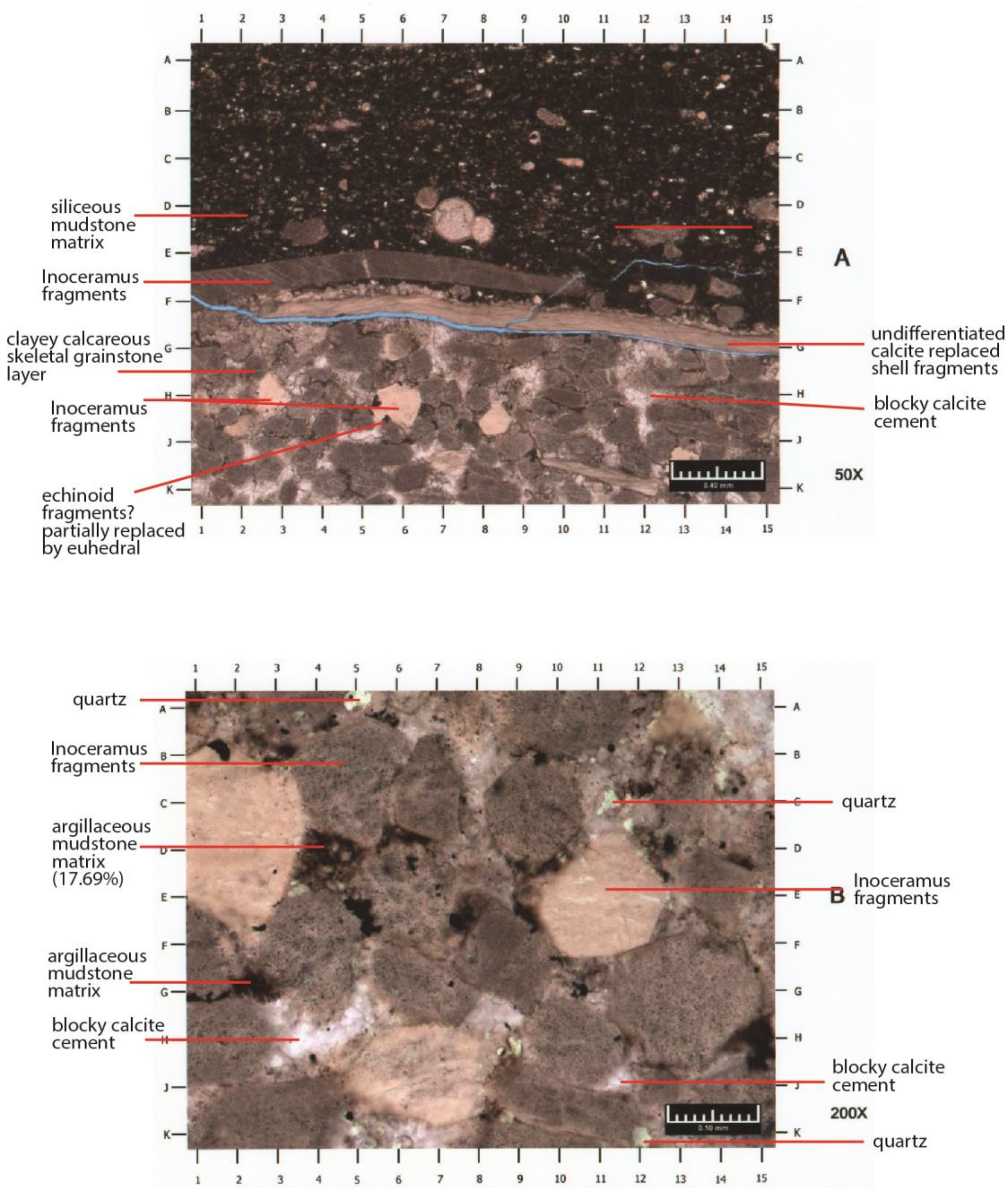

Figure 27: Thin sections obtained from Weatherford Laboratories (2010) show that these grainstone layers are primarily composed of *Inoceramus* fragments, bivalve fragments, foraminifer tests, and phosphatic (fish) particles.

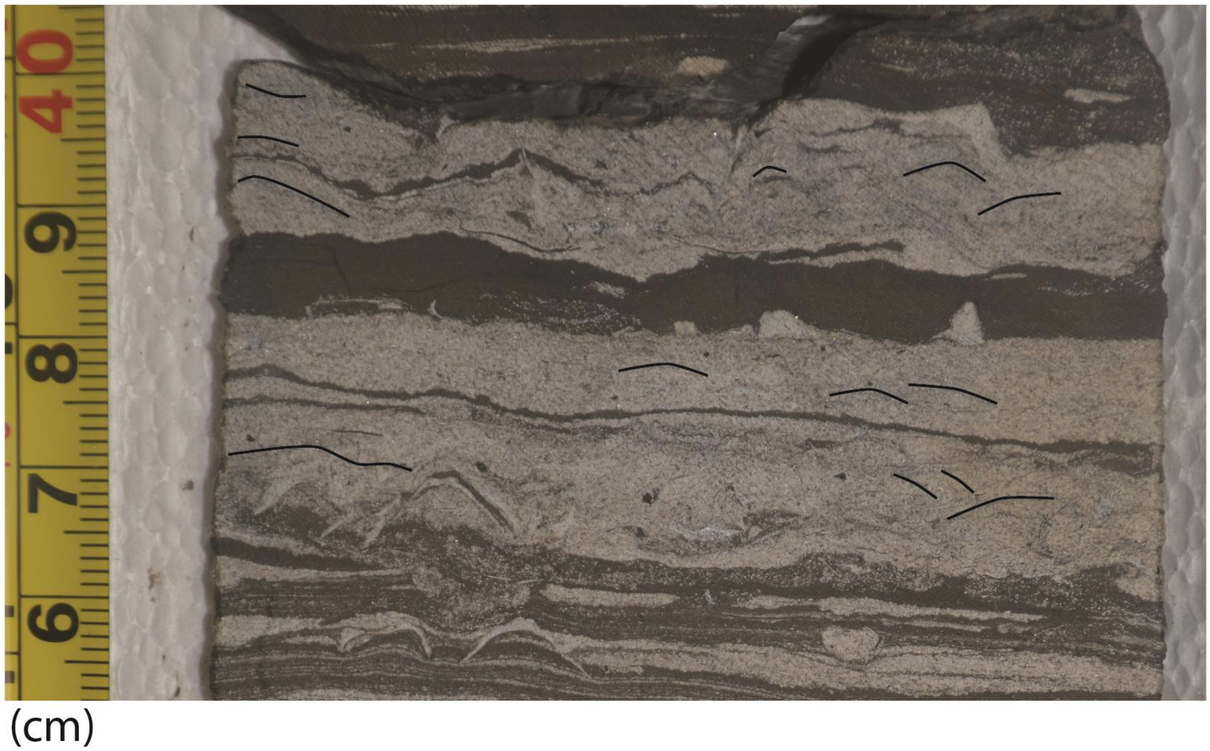

Figure 28: Carbonate skeletal grainstone layers, at a depth of 6920.8 ft. Line drawing highlights foresets dipping in two directions indicating oscillatory wave motion.

Facies 11: Nodules

Three nodules are present throughout the Mancos C core (figure 29). The thicknesses of these units are 13.8 cm in parasequence 1, 16.6 cm in parasequence 2, and 12.5 cm in parasequence 4. The proportion of this facies in each parasequence is 9.7% in parasequence 1, 5.6% in parasequence 2, and 1.9% in parasequence 4.

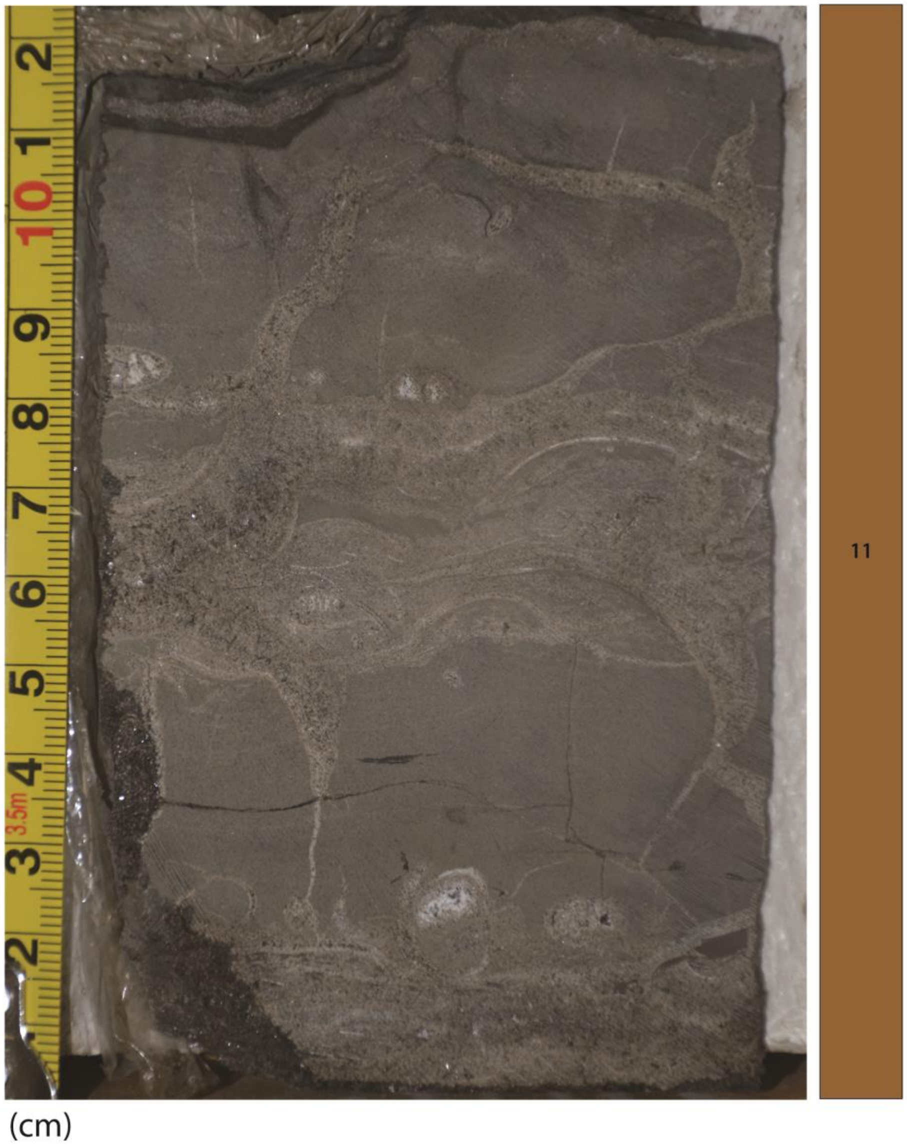

Figure 29: Carbonate nodule with *Inoceramus* fragments, located at a depth of 7198 ft. Correlated facies is included, see figure 8 for facies key.

Facies 12: Bentonite

Four bentonites are present throughout the Mancos C core, with three bentonites being located in the identified parasequences (figure 30). In core, a bentonite is recognized by its light grey/tan colour. Parasequence 2 and 7 both contain one bentonite with a thickness of 0.5 cm (thin lamina). Parasequence 14 has one bentonite with a thickness of 1 cm (very thin bed).

These bentonites only make up a very small portion of their parasequence. The proportion of this facies in paraseqence 2 is 0.18%, parasequence 7 is 1.5%, and parasequence 14 is 0.4%.

Interpretation

Bentonites are layers of volcanic ash that are deposited on the sea floor as a result of a volcanic eruption (Christidis and Huff, 2009). Volcanic ash ejected from a volcano is carried by wind into offshore marine environments where is settles on the seafloor (Christidis and Huff, 2009). Therefore, it is assumed in this study that bentonites are the result of suspension settling.

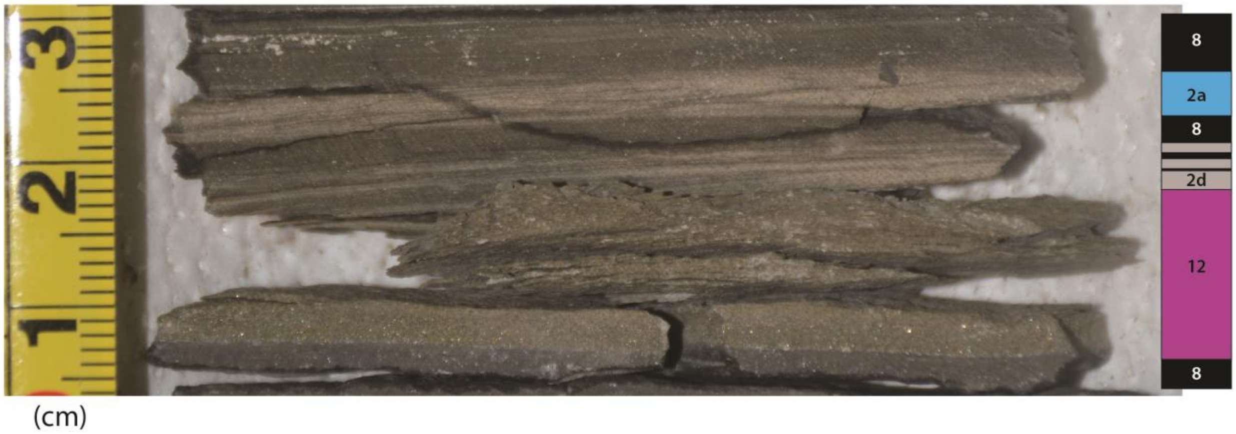

Figure 30: Bentonite layer located, at a depth of 6942.1 ft., with correlated faces. See figure 8 for facies key.

5. Parasequence Analysis

Parasequences were classified based on the proportion of facies that indicate a fluvial fed-, storm wave-, or tide-dominated process (tables 1 and 2). This allows for the determination of the amount of fluvial, wave, or tide influence within a parasequence. A mixed depositional processes is interpreted to represent 50% wave influence and 50% fluvial influence. Facies associations are assigned to the vertical succession of facies to indicate their formative process. A facies key associated with all parasequences is presented in figure 8. Refer to figure 31 for a detailed stratigraphic log of all parasequences.

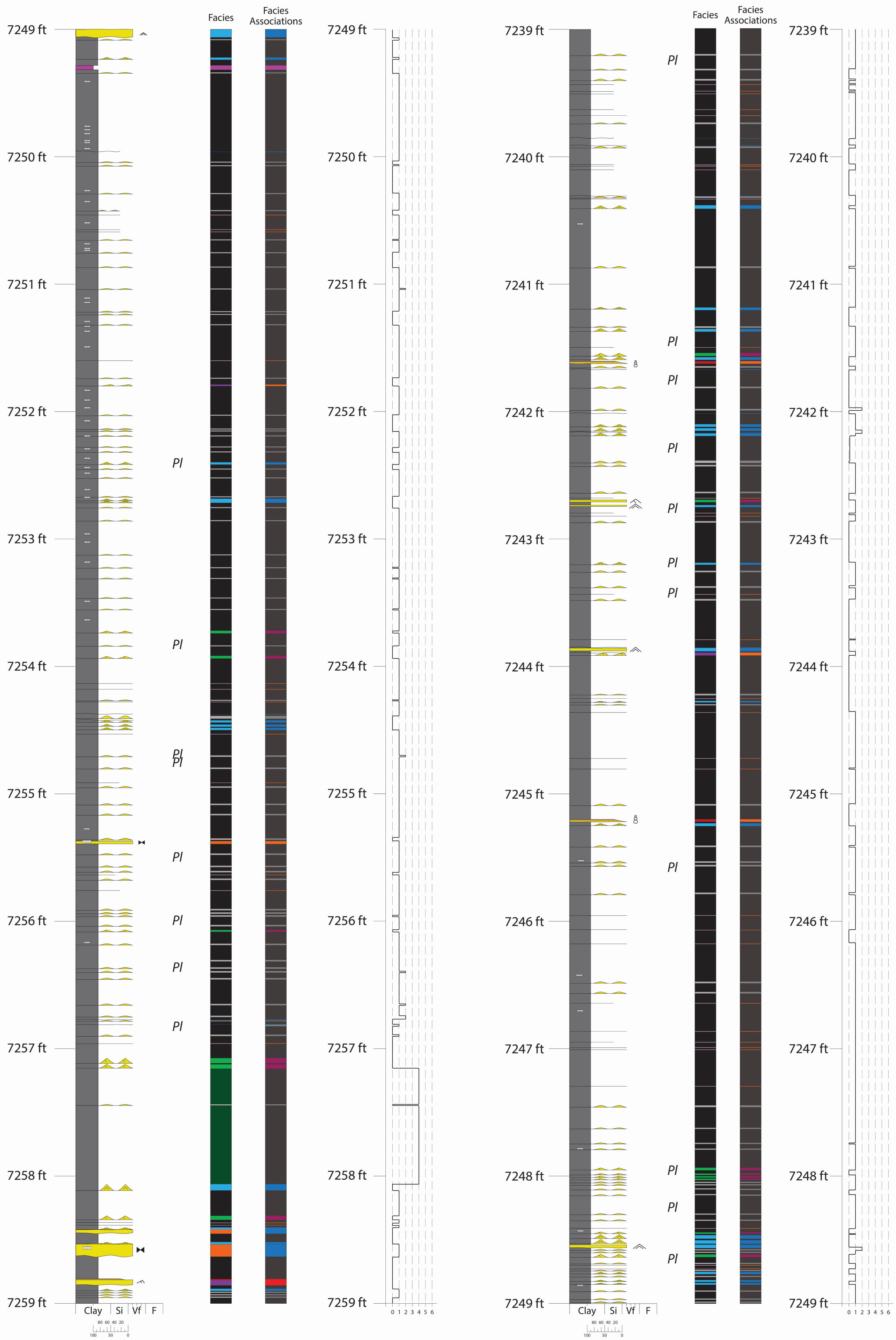

Figure 31: Detailed stratigraphic log of Mancos C, with identified parasequences. Facies associations are assigned to facies. Refer to figure 8 for a facies key.

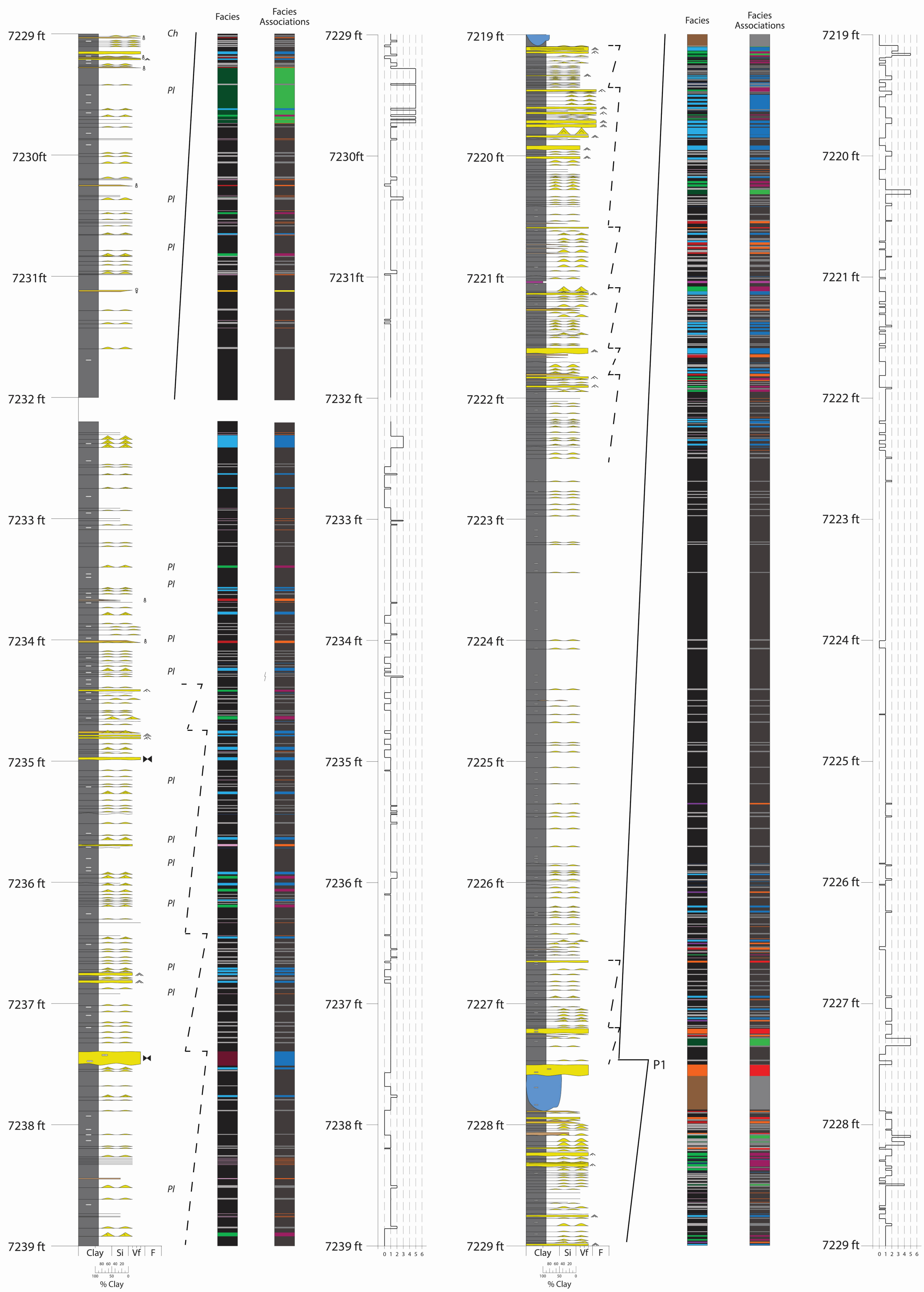

Figure 31 continued: Detailed stratigraphic log of Mancos C, with identified parasequences. Facies associations are assigned to facies. Refer to figure 8 for a facies key.

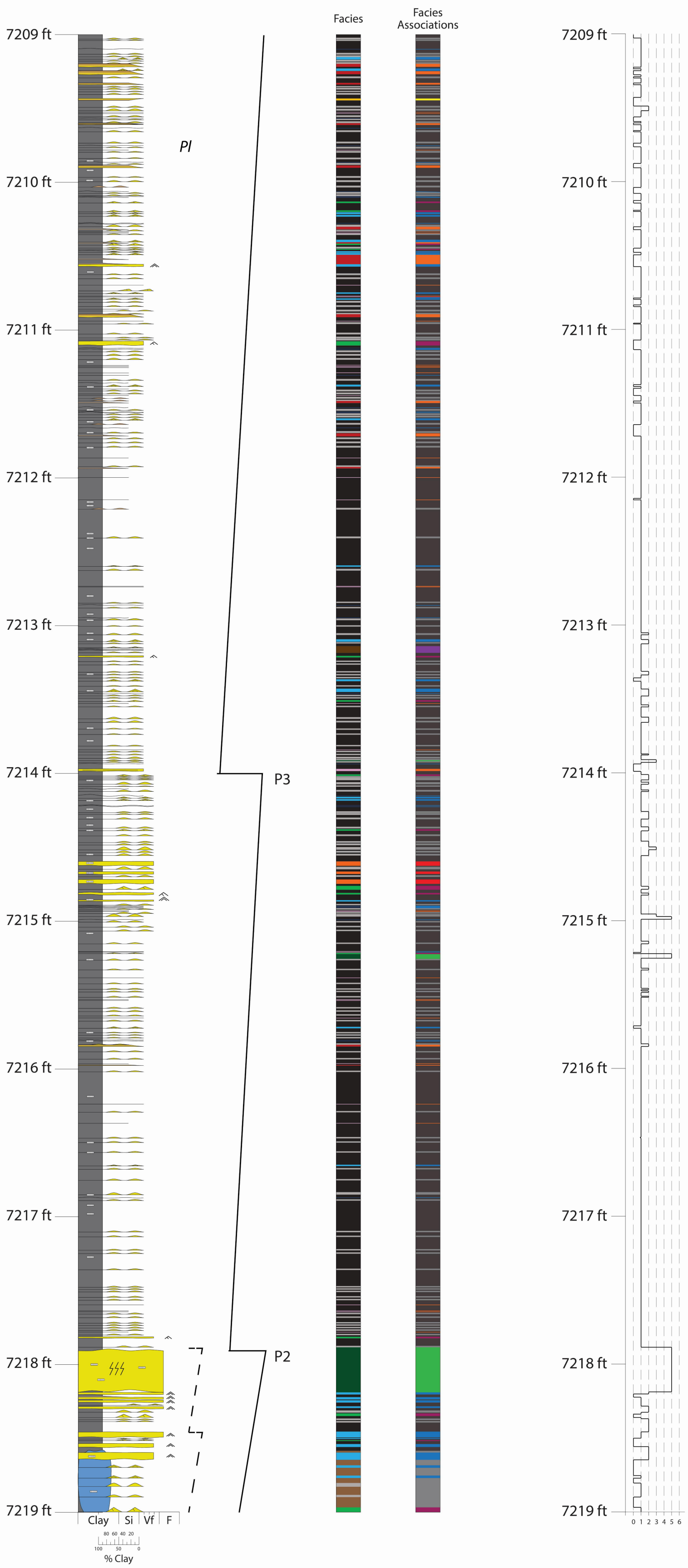

Figure 31 continued: Detailed stratigraphic log of Mancos C, with identified parasequences. Facies associations are assigned to facies. Refer to figure 8 for a facies key.

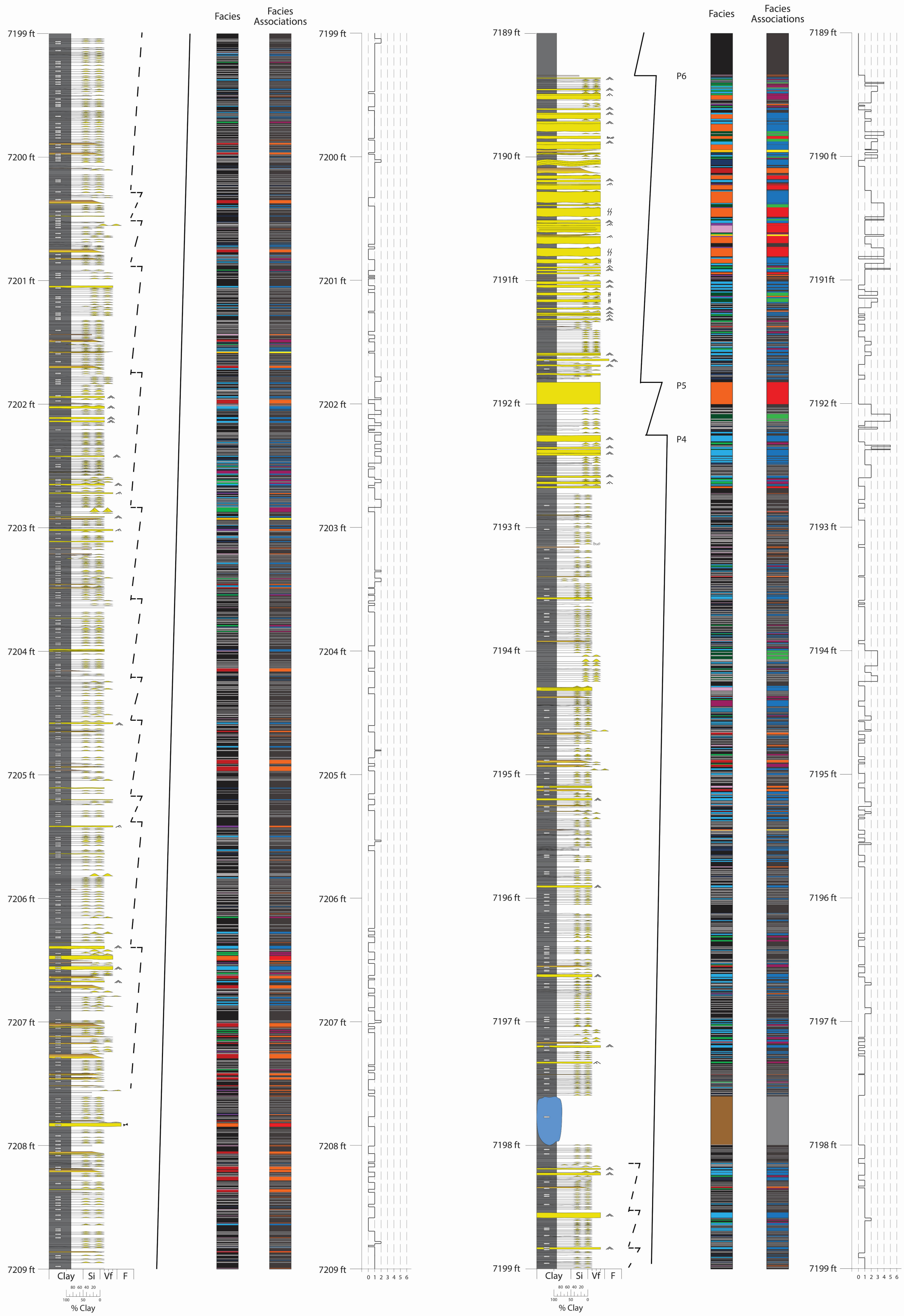

Figure 31 continued: Detailed stratigraphic log of Mancos C, with identified parasequences. Facies associations are assigned to facies. Refer to figure 8 for a facies key.

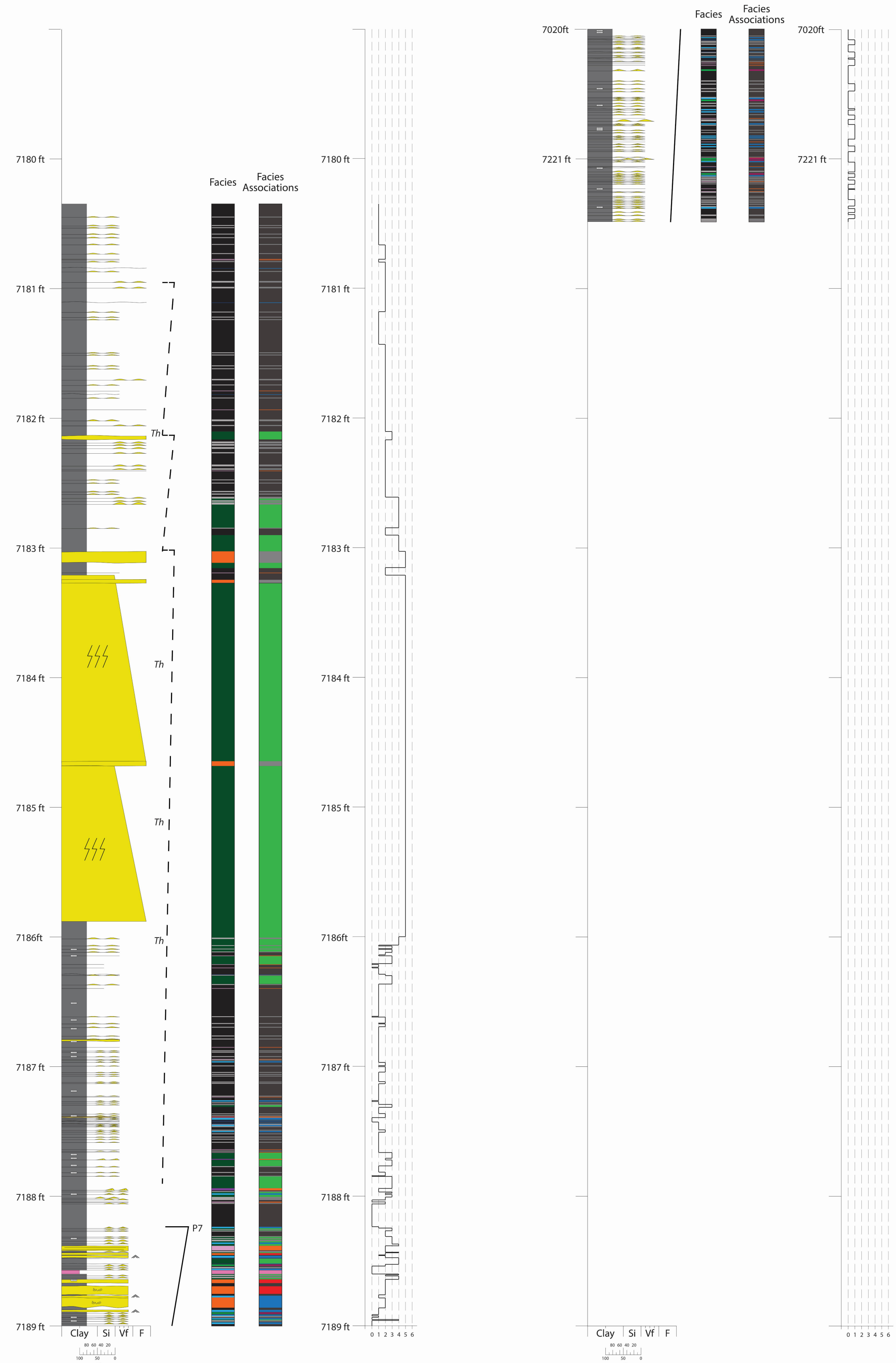

Figure 31 continued: Detailed stratigraphic log of Mancos C, with identified parasequences. Facies associations are assigned to facies. Refer to figure 8 for a facies key.

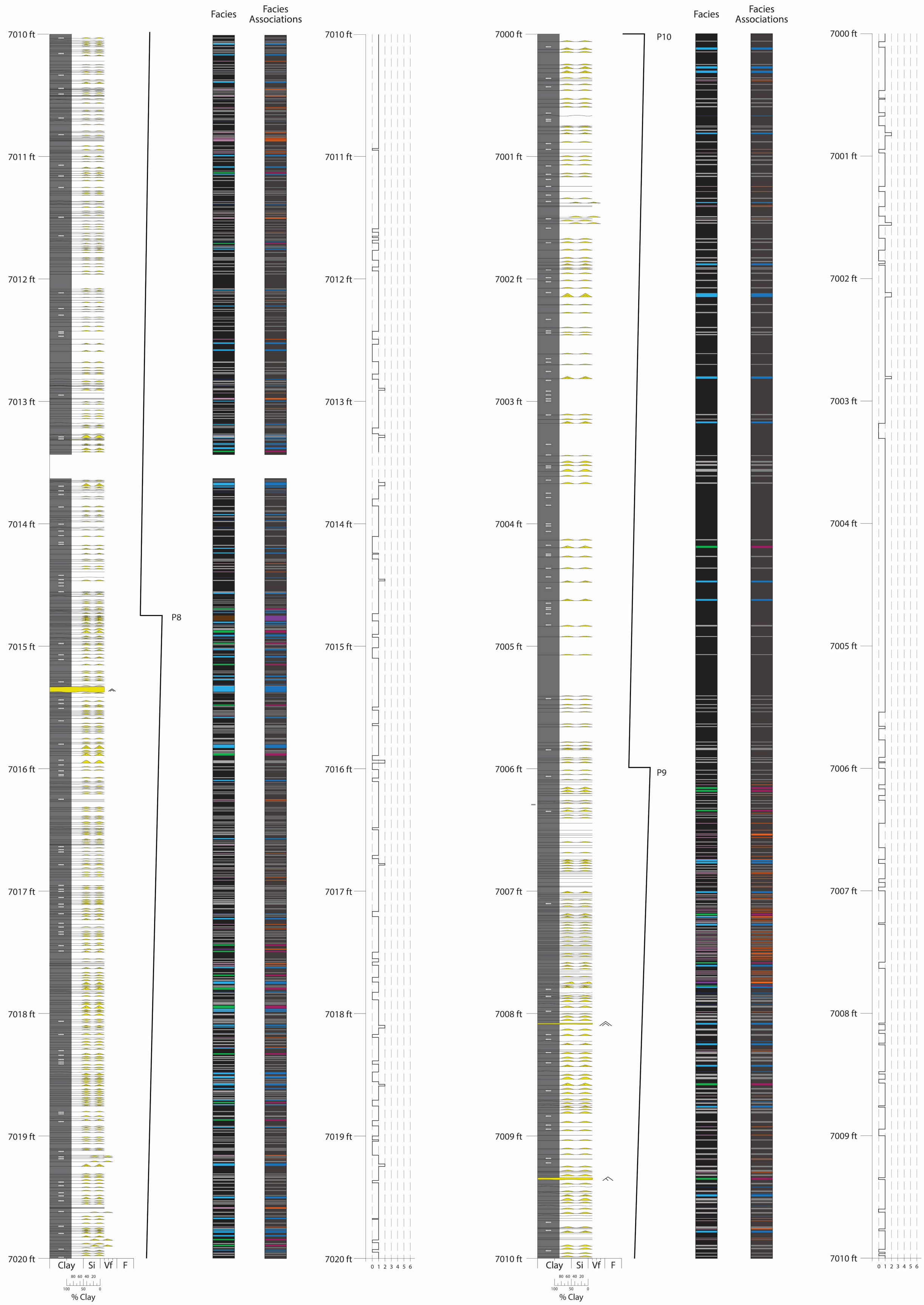

Figure 31 continued: Detailed stratigraphic log of Mancos C, with identified parasequences. Facies associations are assigned to facies. Refer to figure 8 for a facies key.

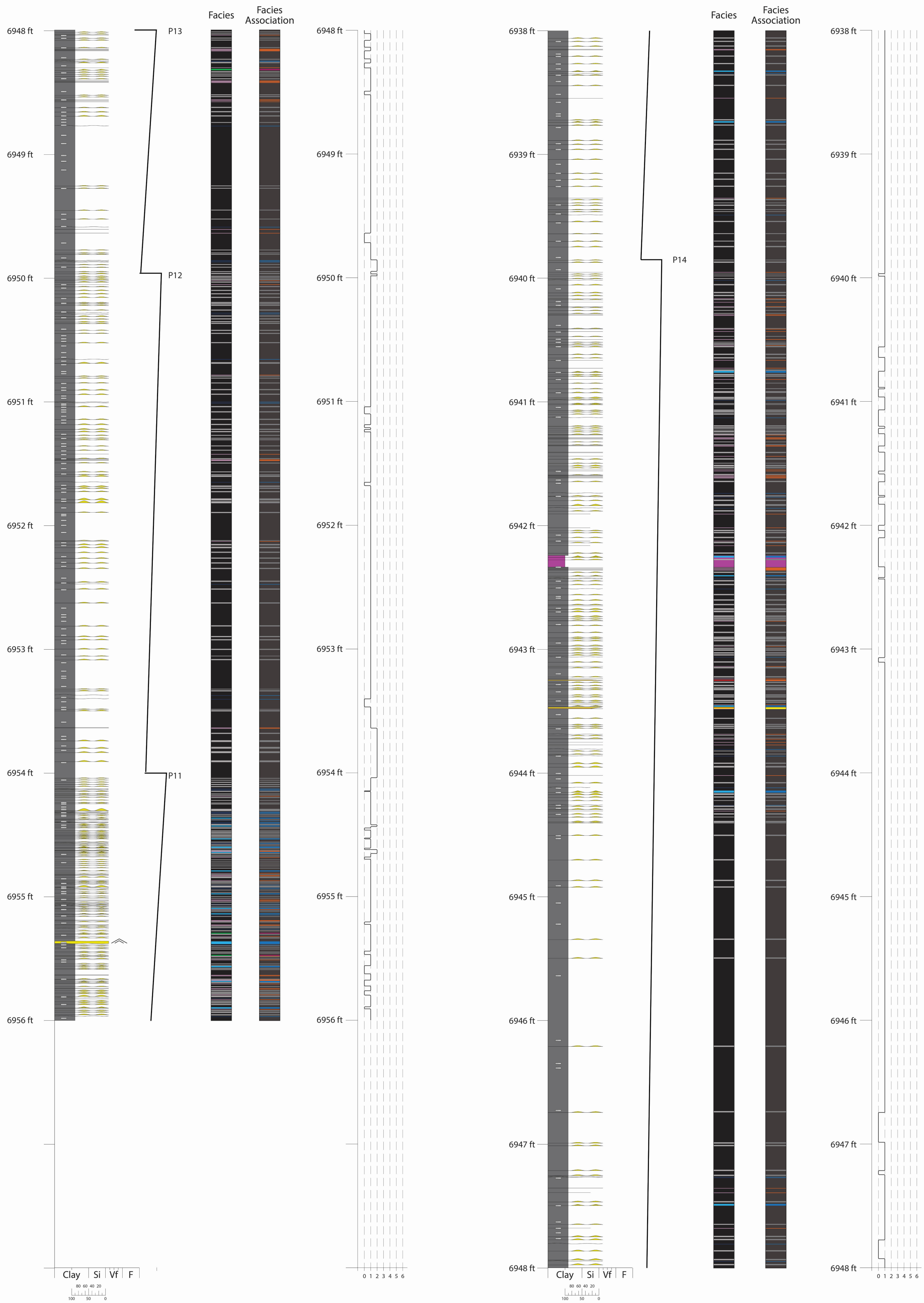

Figure 31 continued: Detailed stratigraphic log of Mancos C, with identified parasequences. Facies associations are assigned to facies. Refer to figure 8 for a facies key.

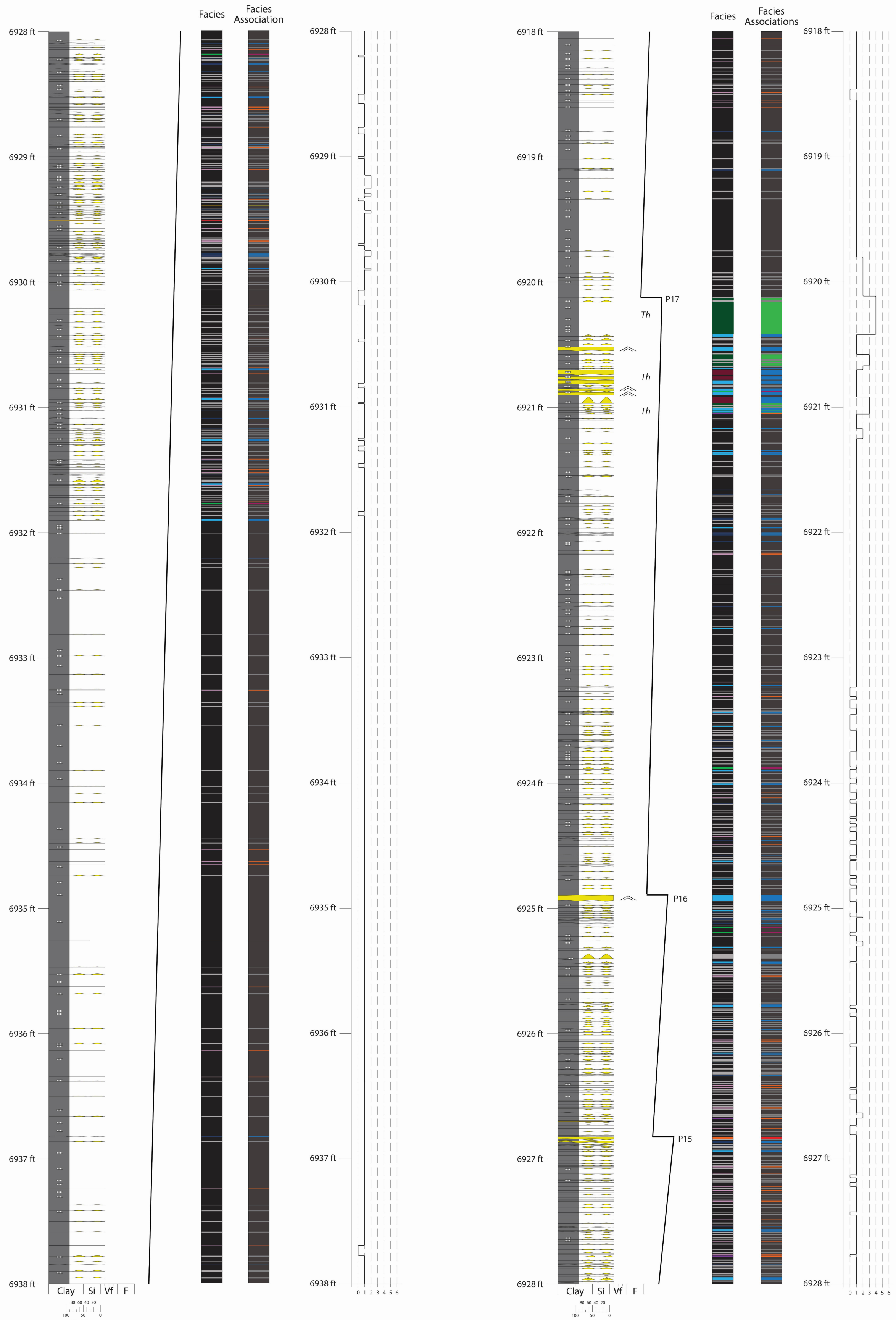

Figure 31 continued: Detailed stratigraphic log of Mancos C, with identified parasequences. Facies associations are assigned to facies. Refer to figure 8 for a facies key.

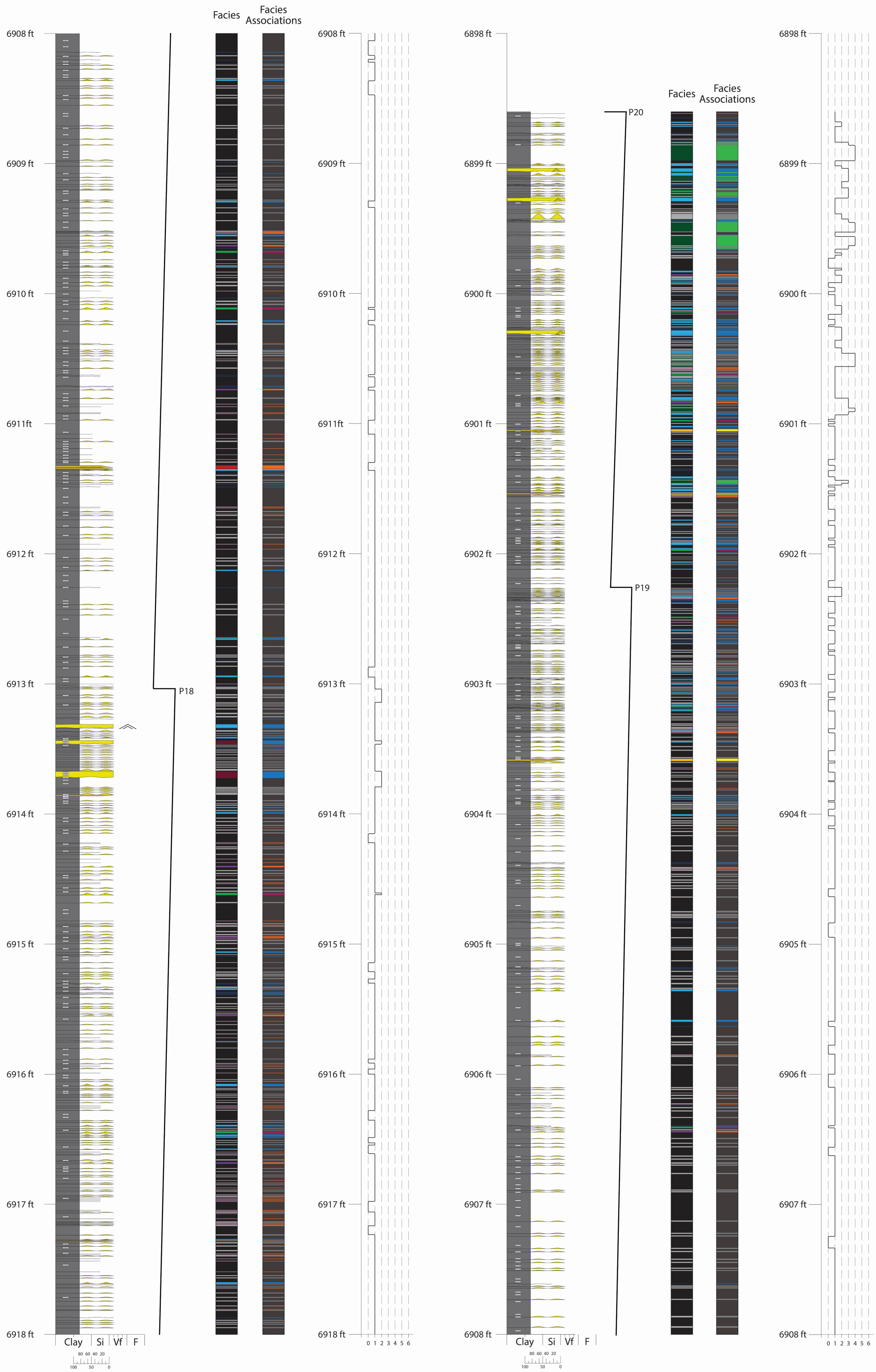

Figure 31 continued: Detailed stratigraphic log of Mancos C, with identified parasequences. Facies associations are assigned to facies. Refer to figure 8 for a facies key.

Table 1: Facies recorded in this study and the relative percentage of each generated by fluvial, wave, and tide-dominated processes

Facies	Depositional Process	P1 (%)	P2 (%)	P3 (%)	P4 (%)	P5 (%)	P6 (%)	P7 (%)	P8 (%)	P9 (%)	P10 (%)	P11 (%)	P12 (%)	P13 (%)	P14 (%)	P15 (%)	P16 (%)	P17 (%)	P18 (%)	P19 (%)	P20 (%)
1) Bioturbated	Fluvial-fed	9.5	4.1	1.3	0.53	11.8	7.6	11.5	-	-	-	-	-	-	-	-	-	7.6	-	-	15.8
2a) Wave ripple	Storm wave	4.4	10.3	2.8	8.1	-	21.1	7.8	7.1	4.0	1.1	3.7	-	-	0.35	0.91	5.0	4.8	1.6	1.2	9.5
2b) Current ripple	Fluvial-fed	1.6	0.64	0.27	0.44	-	4.9	0.25	1.6	1.3	-	-	-	-	-	0.038	0.21	0.12	0.29	0.076	0.40
2c) Combined-flow ripple	Mixed	2.5	1.9	0.95	2.0	-	5.1	2.0	1.5	0.60	0.19	0.33	-	0.25	0.030	0.057	0.26	0.46	0.21	0.29	0.58
2d) Starved ripple	Unknown	6.0	6.1	10.4	17.0	24.7	13.8	9.0	6.5	14.0	8.9	14.4	7.1	5.7	5.6	6.2	17.8	8.9	8.5	3.1	13.4
3) Planar lamination	Fluvial-fed	1.3	0.54	0.84	1.4	-	2.9	0.61	0.73	1.8	0.18	3.5	0.93	1.5	1.5	1.5	2.1	1.3	0.74	0.54	0.30
4) Wavy lamination	Storm wave	0.62	1.0	1.6	3.9	3.2	6.5	2.8	1.3	1.4	0.055	3.1	0.99	0.63	0.64	1.3	3.7	1.6	0.77	1.2	4.3
5) Normal grading	Fluvial-fed	1.3	1.3	0.38	3.1	-	0.40	-	-	-	-	-	-	-	0.010	0.076	-	-	0.047	0.34	-
6) Inverse grading	Fluvial-fed	0.32	-	-	0.19	-	2.2	-	-	-	-	-	-	-	0.015	-	-	-	0.10	0.15	-
7) Structureless sandstone	Fluvial-fed	0.53	0.81	2.2	0.70	45.0	15.5	21.7	-	-	-	-	-	-	-	0.13	-	-	-	-	-
8) Structureless mudstone	Storm wave	62.2	67.4	73.8	60.4	15.3	17.9	32.4	69.3	76.9	89.6	75.0	91.0	91.8	91.5	89.6	70.8	75.5	86.6	93.1	60.6
9) Tidal laminite	Tidal	-	-	0.84	0.29	-	-	-	0.54	-	-	-	-	-	-	-	-	-	-	-	-
10) Grainstone	Wave	-	-	-	-	-	-	-	-	-	-	-	-	-	-	-	-	2.0	1.2	-	-
11) Nodules	Biogenic	9.7	5.7	-	1.9	-	-	-	-	-	-	-	-	-	-	-	-	-	-	-	-
12) Bentonite	Suspension settling	-	0.2	-	-	-	-	1.5	-	-	-	-	-	-	0.40	-	-	-	-	-	-
Parasequence Thickness (m)		1.4	2.9	1.2	6.60	0.13	0.76	0.33	2.1	2.6	1.8	0.61	1.2	0.59	2.50	4	0.58	1.5	2.2	3.3	1.1

Table 2: Fluvial versus wave versus tide dominance in each parasequence

	P1 (%)	P2 (%)	P3 (%)	P4 (%)	P5 (%)	P6 (%)	P7 (%)	P8 (%)	P9 (%)	P10 (%)	P11 (%)	P12 (%)	P13 (%)	P14 (%)	P15 (%)	P16 (%)	P17 (%)	P18 (%)	P19 (%)	P20 (%)
Fluvial-fed	14.5	7.5	5.0	6.5	56.9	37.1	46.0	2.3	3.0	0.18	3.5	0.93	1.5	1.5	1.7	2.4	9.0	1.2	1.1	17.2
Storm wave	67.3	78.7	78.2	72.4	18.4	45.6	43.0	77.6	82.3	90.7	81.8	92.0	92.5	92.5	91.8	79.6	83.9	90.1	95.4	74.4
Mixed	2.5	1.9	0.95	2.0	-	5.1	2.0	1.5	0.6	0.19	0.33	-	0.25	0.03	0.06	0.26	0.46	0.21	0.29	0.58
Tidal	-	-	0.84	0.29	-	-	-	0.54	-	-	-	-	-	-	-	-	-	-	-	-
Biogenic	9.7	5.7	-	1.9	-	-	-	-	-	-	-	-	-	-	-	-	-	-	-	-
Suspension settling	-	0.18	-	-	-	-	1.5	-	-	-	-	-	-	0.40	-	-	-	-	-	-
Unknown	6.0	6.1	10.4	17.0	24.7	13.8	9.0	6.5	14.0	8.9	14.4	7.1	5.7	5.6	6.2	17.8	8.9	8.5	3.1	13.4
Classification	Wf	Wf	Wf*t*	Wf*t*	Fw	Wf	Fw	Wf*t*	Wf	Wf	Wf	Wf	Wf	Wf*t*	Wf	Wf	Wf	Wf	Wf	Wf

5.1 Parasequence Description and Interpretation

All of the parasequences, except for parasequences 5 and 7, are storm wave-dominated and fluvial-influenced (Wf). Structureless mudstone is the dominant facies within each of these parasequences. Frequent storms were likely responsible for resuspending mud and allowing it to move further offshore as a fluid mud, thus giving this structureless mudstone a storm wave-dominance. Fluvial influence within the wave-dominated, fluvial influenced parasequences is evident from facies such as bioturbated units, current ripples, planar laminations, normal and inverse grading, and structureless sandstone. Since the core is located about 137 km offshore, these facies would have initially been brought offshore by fluvial influences, however storms and waves were responsible for the transport of these sediments further into the basin. Bioturbated units could be the result of slow suspension settling from hypopycnal flows, which would allow enough time for colonization. Current ripples, planar laminations, normal grading, and structureless sandstone are all capable of being produced by ignitive turbidites and hyperpycnal flows. Within this core it is difficult to discern which facies belong to which process, since full turbidite and hyperpycnite deposits are not preserved. Inverse grading, however, can be attributed to hyperpycnal flows. Three parasequences, 3, 4, and 8, show evidence of possible tidal rhythmites. Therefore, these parasequences can be classified as wave-dominated, fluvial-influenced, and tidally affected (Wf*t*).

Parasequence 5 is fluvial-dominated and storm wave-influenced. This parasequence is also the thinnest (0.13 m), making percentages seem higher than normal. Structureless sandstone and bioturbated units are the main fluvial influences within the parasequence, while structureless mudstone and wavy laminations are the main storm wave influences. Again, fluvial influence can be attributed to either ignitive turbidites, hyperpycnal or hypopycnal flows, that are fed by fluvial river sediment.

Parasequence 7 shows mixed fluvial (46%) and storm wave (43%) influence, with structureless mudstone being the dominant facies within the parasequence.

6. Discussion

6.1 Parasequence Variability

In this study, parasequences within different systems tracts can be compared. Multiple systems tracts were identified in the core and can be seen in figure 5. Lowstand systems tracts (7192.7 to 7196.1 ft and 6903.6 to 6898.6 ft) show coarser grains and thicker laminations, indicating slow sea level fall. Above the LST a transgressive surface is found. Above the first transgressive surface is a bioturbated, fine upper, glauconitic sandstone. This unit is thought to correlate with the Tocito sandstones, which are the primary oil reservoirs in the San Juan Basin (Ridgley et al., 2013). Dominant burrows in both transgressive systems tracts include *Thalassinoides*. Highstand systems tracts (7259 to 7192.7 ft and 6916.2 to 6903.6 ft) lie above the maximum flooding surface and show parasequences with finer grains and thinner laminations.

6.2 Frequency of events

The Mancos C was deposited during the middle Coniacian to early Turonian (figure 2) and it is assumed that it took approximately 2 myr to deposit (Nummedal and Molenaar, 1995). A total of 10,860 beds were measured within Mancos C, therefore there is an average frequency of 184 years between events. This is a large time gap between events, considering the lack of bioturbation throughout the core. It is likely that this time is associated with flooding surfaces, where bioturbation tends to increase. In terms of parasequence cyclicity, 20 parasequences were observed within the core, suggesting an average frequency of 100 kyr for the 20 parasequences. This cyclicity frequency potentially represents Milankovitch cycles.

6.3 Variability between thin beds and the importance of mud depositional processes

The depositional processes responsible for the formation of thin beds, as discussed earlier, are important to understanding shale geophysics (Hart et al., 2013). These processes are able to (1) control the minerology, porosity, organic content, and fabric of mudstones; (2) control lateral and vertical heterogeneity; (3) control the thickness of mudstone successions (Hart et al., 2013). These properties are important for understanding source-rock reservoirs because they have a control on hydrocarbon type and volume, porosity, and permeability (Hart et al., 2013). They also have a control on how rocks will respond to hydraulic fractures, and how seismic waves will reflect off of beds (Hart et al., 2013).

At the lamina scale (micrometer to millimeters) mudstones are often anisotropic, meaning that they change faster vertically than they do laterally (Hart et al., 2013). This anisotropy is associated with lamina that have variations in grain size, mineralogy, and or porosity (Hart et al., 2013). These variations can all be attributed to processes such as ignitive turbidites, hypopycnal and hyperpycnal flows, tempestites, tides, and fluid muds. In the case of this study, grain sizes vary vertically but not all of the time. Isotropy can exist in mudstones at this scale, which include bioturbated deposits and some suspension deposits (Hart et al., 2013). It is, however, difficult to measure the lateral extent of laminations, especially in core. Only well exposed outcrops allow millimeter-scale laminations to be traced out laterally over only a few meters (Hart et al., 2013).

Anisotropy is also present at bed and bedset scale (several centimeters to several meters), due to the interbeding of mudstones with other lithologies (Hart et al., 2013). At the bed and bedset scale, anisotropy is due to the interbedding of mudstones with other lithologies (Hart et al., 2013).

In this study, the Mancos C core can be broken down into three major facies: (1) laminated mudstone (mm scale); (2) very thin bedded mudstone (cm scale); and (3) structureless mudstone. The three facies show anisotropy at a larger scale, similar to the bed and bedset scale disscused by Hart et al. (2013). However, the focus of this study was on lamina scale (mm to cm scale) heterogeneity, which is evident throughout the core. Moving up a parasequence, there are a variety of different sedimentary structures deposited from processes such as ignitive turbidites, hyperpycnites, and tempestites. Some facies are present in stacking patterns such as inverse and normal grading, Bouma Sequences, and tempestite sequences. Others are seen as single laminations, such as wave ripples, combined-flow ripples, current ripples, planar and wavy laminations.

On average, storm wave-driven processes comprise approximately 75% of the Mancos C core. In contrast, fluvial-fed driven processes comprise, on average, 11%. The average percentages of current ripples (0.9%) and combined-flow ripples (1%) are minor compared to those of wave ripples (5.5%). This indicates that fair weather waves had no influence on deposition, therefore deposition occurred below fair weather wave base, but above storm wave base. Structureless mudstone is the dominant facies throughout the entire Mancos C core, averaging 70%, meaning that inner shelf mud processes, such as wave resuspension of mud, played a key role in moving sediment further offshore. The lack of evidence for the tripartite divisions of WESGFs suggests that this process was not dominant within the Mancos C core.

Fluvial-influenced processes, such as ignitive turbidites and hyperpycnal flows, proved to be difficult to distinguish from one another. This is because both hyperpycnal flows and ignitive turbidites are capable of depositing normally graded beds once their flow wanes. Also, depending on the magnitude of the flood, the entire inversely graded unit of a hyperpycnite can be fully eroded before the deposition of a normally graded unit (Mulder and Alexander, 2001). Full successions of ignitive turbidite are rarely preserved. In this study, Bouma T_B-T_C and T_D-T_E sequences were locally observed (figure 15). Certain sedimentary structures can be produced by multiple depositional processes. For example, current ripple laminations can be produced from either ignitive turbidity currents or hyperpycnal flows (Li et al., 2015). Both indicate unidirectional flow and therefore does not impact whether the setting of deposition is fluvial or wave. The only distinctive characteristic separating hyperpycnites and turbidity currents is the inverse grading found in hyperpycnites as a result of waxing flow. This allowed for the confident conclusion that these inversely graded beds could be assigned to hyperpycnal flows.

Some of the bioturbated units within the Mancos C core show evidence of cryptobioturbation (figure 9). Crypobioturbation is caused by subtle biogenic disturbances, such as micro borings, bacterial trails, meiofaunal burrows, etc. (Pemberton et al., 2008). In fine-grained sediments, cryptobioturbation is produced in marine and freshwater environments (Pemberton et al., 2008). These units looked homogeneous at first glance, but with image enhancement small burrows could be picked out, however the type of burrow could not be determined. Because these units are highly reworked, creating an almost massive appearance, it is likely that there was slow deposition of sediment to allow cryptobioturbation to occur (MacEachern et al., 2005). The trace fossils that are clearly seen in other sections of the core, such as *Planolites, Chondrites,* etc., are isolated and occur in small amounts. This lack of diversity may indicate a storm flood dominance. Storm floods are short-lived increases in discharge from small rivers, as the result of extreme rainfall events (Wheatcroft, 2000). The high sediment discharge, produced by these floods, enters the ocean and can subsequently be reworked and distributed by oceanic processes (Wheatcroft, 2000). It is possible that these storm floods may have created stressed conditions for certain organisms to live, therefore, leading to a lack of diversity in the type of burrows found within the Mancos C core.

6.4 Relationship with current depositional facies models

The results of this study can be compared to a mudstone facies model developed by Hart (2016) (figure 32). This model links sedimentary processes and their depositonal products in a large epicontinental basin (Hart, 2016). Proximal areas should be dominated by siliciclastic mudstones interbedded with sandstone beds deposited by bottom flows, such as turbidity currents, hyperpycnal flows, tempestites, and WESGFs (Hart, 2016). With increasing distance from the shoreline, mudstones become enriched in biogenic components such as planktonic foraminifera (Hart, 2016). As sea level and sediment supply changes, these facies can shift laterally, expand, or shrink (Hart, 2016).

The Mancos C core was located 137 km offshore and deposited within a water depth of < 100 m. Therefore, the San Juan Basin shelf had a slope of approximately 0.04^{o} (absolute value: 7×10^{-4}). This slope is too shallow for purely hyperpycnal flows or turbidity currents to transport sediment across the shelf (figure 1). Storm waves and tides would have aided these processes, allowing them to travel down a slope of 0.04^{o}, and carry them up to 137 km offshore. Clastics dominate within the core making up more than 95%, while carbonate grainstones make up less than 5%. This indicates that deposition within the Mancos C core is quite proximal, taking place between zones 1 and 2 of Hart's facies model (figure 32).

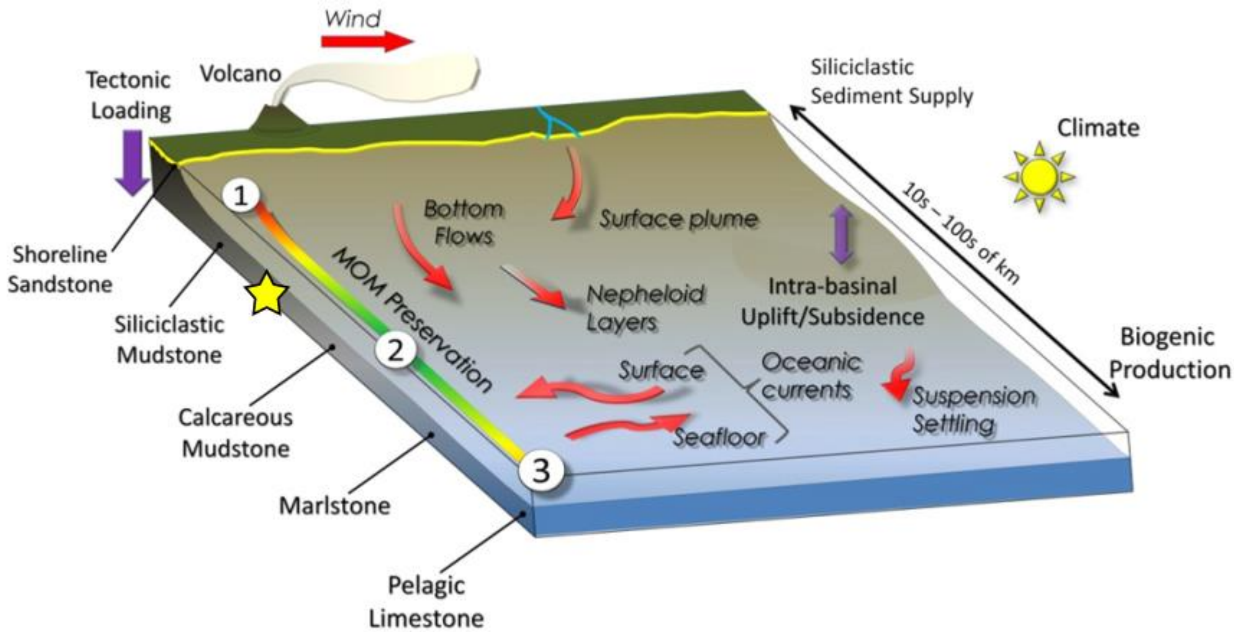

Figure 32: Mudstone/source rock deposition model in an epicontinental seaway. Red arrows represent processes that deposit sediment. Proximal deposits are dominated by shorelines sandstones. Proximal mudstones are dominated by siliclastic components such as clay and quartz silt). The proportion of biogenic sediments, such as planktonic calcite, increases further offshore. Marine organic matter (MOM) presevation is represented in three main zones. Zone 1 is dominated by siliclastic mudstones with a low preservation for MOM. Zone 2 is dominated by calcareous mudstones that have good preservation potential for MOM. Zone 3 is dominated by pelagic limestones with low MOM content (taken from Hart, 2016). The yellow star indicates the approximate location of deposition in the Mancos C core.

6.5 Comparison of thin-bedded facies in core

Facies from the Mancos C core can be compared to other delatic systems. Plint (2014) created thin sections from prodelatic core of the Dunvegan to determine the origin of different grain types and the possible transport processes bringing mud offshore. Using thin sections, Plint (2014) was able to measure mm scale beds and identify microfacies. Rippled microfacies (figure 33) look very similar to those found within the Mancos C core. As well, siltstone lamination thicknesses within Plint's core range from 0.1 mm to 1 cm. These thicknesses show a resemblance to siltstone and sandstone laminations found within the Mancos C core, which range from 0.1 mm to 3 cm. This shows that a well preserved core can provide almost the same level of detailed facies as those found in thin sections. Thin sections and the use of SEMs would be useful to identify the composition of the mudstone and types of grains (e.g., flocs, rip-up clasts, pyrite framboids) within the Mancos C core.

Like the Mancos C core, within the Dunvegan core there is great vertical variability, indicating a very dynamic depositional environment (Plint, 2014). Plint (2014) tried to correlate between stratigraphic thin sections, spaced 20 mm apart, which proved to be difficult. Extreme lateral variability could be observed between thin sections due to the lateral change in thickness of microfacies and the millimeter scale erosion at the base of the beds (Plint, 2014). Since only one core was observed in this thesis, a correlation could not be done. However, it is hypothesized that there would be great lateral variability between cores since there is vertical variability within the Mancos C core.

6.6 Importance and application for future studies

Previous studies have not looked at the Mancos Shale in the same level of detail as this study. These studies provide broad descriptions for the Mancos Shale, and regional cross sections of the Mancos Shale display the unit as being made up of just clay or silt (Molenaar, 1973, 1977; Nummedal and Molenaar, 1995). There is no indication of any interbedded sandstone laminations and therefore no indication of the types of facies found within the Mancos Shale. Molenaar (1977) describes the Mancos Shale as being deposited in deeper, quieter water in offshore areas with low energy levels. This is not the case in Mancos C, of the Upper Mancos Shale, as it is a storm-dominated environment where wave action helps to deposit clay and silt. Therefore, detailed facies analysis is critical to understand the type of environment that the Mancos Shale was deposited in, which helps to update what previous studies have concluded about the Mancos Shale.

Facies analysis of other Mancos Shale cores could be done at a less detailed scale (i.e., not measuring every lamination), however the percentages of each facies would have less accuracy. Grouping a number of laminations together would either cause an overestimation or underestimation of that facies. This would also affect the accuracy of whether the environments within each parasequence are wave-, fluvial, or tide-dominated. Perhaps, some type of computer automation could help to pick out sandstone versus shale layers and measure their thicknesses. This would greatly reduce the amount of time when analyzing the core. Doing a detailed facies analyis by measuring each lamination ensures the most accurate measurement of each facies and their depositional process.

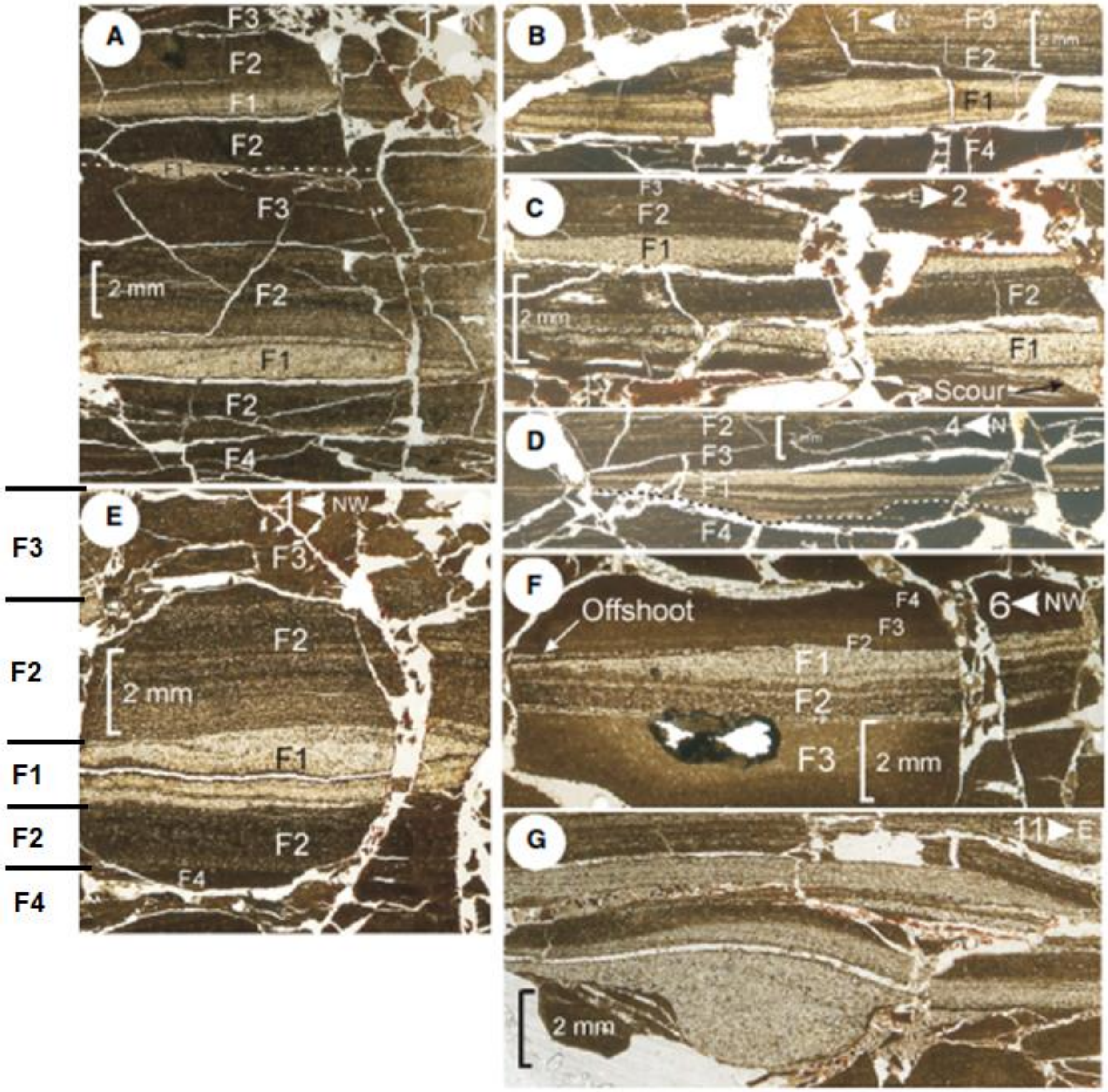

Figure 33: Well-sorted rippled sandstone from thin-bedded deposits of the Dunvegan formation. Rippled or structureless well-sorted siltstone (F1); silt-streaked claystone (F2); structureless silty claystone (F3); clay-rich mudstone (F4). All images are from thin section scans (taken from Plint, 2014).

7. Conclusions

Mancos C of the Upper Mancos Shale exhibits a variety of different facies produced by a number of depositional processes. Storm wave-driven processes comprise 75% of the core compared to fluvial-fed driven processes, which make up only 11%. The proportion of wave ripples (5.5%) is greater than that of current (0.9%) and combined-flow ripples (1%), indicating that deposition occurred below fair weather wave base, but above storm wave base. The dominant facies throughout the entire Mancos C core was structureless mudstone (70%). This indicates that inner shelf mud processes, such as wave resuspension of mud, played a key role in moving sediment up to 137 km offshore. Gravity driven processes such as hyperpycnal flows, tempestites, and turbidites, as well as hypopycnal flows and wave modified flows, also contributed to the movement of these muds within the Cretaceous Western Interior Seaway, however, only for short distances.

Overall, the analysed core was located proximal to the shoreline, falling between zones 1 and 2 of Hart's epicontinental facies model. This is evident from the high percentage of clastic sediments (95%), compared to carbonates (5%).

Detailed thin-bedded analysis of well preserved core is able to produce similar results as thin-bedded studies conducted using thin sections, allowing large sections of core to be analysed, rather than a number of small specific locations.

References

Aigner, T., 1982, Calcareous Tempestites: Storm-dominated Stratification in Upper Muschelkalk Limestones (Middle Trias, SW-Germany), *in* Cyclic and Event Stratification: Berlin, Springer-Verlag, p. 180–195.

Ainsworth, R. B., B. K. Vakarelov, and R. A. Nanson, 2011, Dynamic spatial and temporal prediction of changes in depositional processes on clastic shorelines: Toward improved subsurface uncertainty reduction and management: AAPG Bulletin, v. 95, no. 2, p. 267–297.

Bates, C. C., 1953, Rational Theory of Delta Formation: Bulletin of the American Association of Petroleum Geologists, v. 37, no. 9, p. 2119–2162.

Bentley, S. J., 2003, Wave-current dispersal of fine-grained fluvial sediments across continental shelves: the significance of hyperpycnal plumes, *in* Siltstones, mudstones and shales: Depositional processes and characteristics: SEPM, CD-ROM: p. 35–48.

Bhattacharya, J. P., and J. A. MacEachern, 2009, Hyperpycnal Rivers and Prodeltaic Shelves in the Cretaceous Seaway of North America: Journal of Sedimentary Research, v. 79, no. 4, p. 184–209.

Bouma, A. H., 1962, Sedimentology of some flysch deposits: a graphic approach to facies interpretation: Elsevier Pub. Co.

Broadhead, R. F., 2015, The Upper Mancos Shale in the San Juan Basin: three plays, conventional and unconventional: Search and Discovery, v. 10791, p. 1–39.

Campbell, C. V., 1979, Model for beach shoreline in Gallup Sandstone (Upper Cretaceous) of northwestern New Mexico: New Mexico Bureau of Mines and Mineral Resources, v. Circular 1, p. 1–37.

Christidis, G. E., and W. D. Huff, 2009, Geological aspects and genesis of bentonites: Elements, v. 5, no. 2, p. 93–98.

Correggiari, A., A. Cattaneo, and F. Trincardi, 2005, Depositional Patterns in the Late Holocene Po Delta System: River Deltas-Concepts, Models, and Examples, v. SEPM Speci, p. 365–392.

Dalrymple, R. W., 2010, Tidal Depositional Systems, *in* N. P. James, and R. W. Dalrymple, eds., Facies Models 4: St. John's, Geological Association of Canada, p. 201–231.

Dalrymple, R. W., E. K. Baker, P. T. Harris, and M. G. Hughes, 2003, Sedimentology and stratigraphy of a tide-dominated, foreland-basin delta (Fly River, Papua New Guinea): Special Publication - Society for Sedimentary Geology, v. 76, p. 147–173.

Dosen, K., 2017, Mud Distribution in the Cretaceous Western Interior Seaway: A Thin Bedded Facies Analysis of the Upper Mancos Shale, New Mexico: 66 p.

Duke, W. L., 1990, Geostrophic Circulation or Shallow Marine Turbidity Currents? The Dilemma of Paleoflow Patterns in Storm-Influenced Prograding Shoreline Systems: Journal of Sedimentary Petrology, v. 60, no. 6, p. 870–883.

Friedrichs, C. T., and L. D. Wright, 2004, Gravity-driven sediment transport on the continental shelf: Implications for equilibrium profiles near river mouths: Coastal Engineering, v. 51, no. 8–9, p. 795–811.

Galloway, W. E., 1975, Process Framework for Describing the Morphologic and Stratigraphic Evolution of Deltaic Depositional Systems: Deltas: Models for Exploration, p. 86–98.

Hart, B. S., 2016, Marine mudstone source rocks in epicontinental basins: Development of a conceptual facies model and application to Cenomanian/Turonian mudstones of the Cretaceous Western Interior Seaway, *in* M. P. Dolan, D. K. Higley, and P. G. Lillis, eds., Hydrocarbon Source Rocks in Unconventional Plays, Rocky Mountain Region: p. 364–421.

Hart, B. S., J. H. S. Macquaker, and K. G. Taylor, 2013, Mudstone (“shale”) depositional and diagenetic processes: Implications for seismic analyses of source-rock reservoirs: Interpretation, v. 1, no. 1, p. B7–B26.

He, S., T. K. Kyser, and W. G. E. Caldwell, 2005, Paleoenvironment of the Western Interior Seaway inferred from 18O and 13C values of molluscs from the Cretaceous Bearpaw marine cyclothem: Palaeogeography, Palaeoclimatology, Palaeoecology, v. 217, no. 1–2, p. 67–85.

Ichaso, A. A., and R. W. Dalrymple, 2009, Tide- and wave-generated fluid mud deposits in the Tilje Formation (Jurassic), offshore Norway: Geology, v. 37, no. 6, p. 539–542.

Khan, S. M., J. Imran, S. Bradford, and J. Syvitski, 2005, Numerical modeling of hyperpycnal plume: Marine Geology, v. 222–223, no. 1–4, p. 193–211.

Kineke, G. C. C., R. W. W. Sternberg, J. H. H. Trowbridge, and W. R. R. Geyer, 1996, Fluid-mud processes on the Amazon continental shelf: Continental Shelf Research, v. 16, no. 5–6, p. 667–696.

Kirby, R., and W. R. Parker, 1983, Distribution and behavior of fine sediment in the Severn Estuary and Inner Bristol Channel, U.K.: Canadian Journal of Fisheries and Aquatic Sciences, v. 40, p. 83–95.

Kneller, B. C., and M. J. Branney, 1995, Sustained high-density turbidity currents and the deposition of thick massive sands: Sedimentology, v. 42, no. 4, p. 607–616.

Kvale, E. P., 2006, The origin of neap-spring tidal cycles: Marine Geology, v. 235, p. 5–18.

Lamb, G., 1968, Stratigraphy of the Lower Mancos Shale in the San Juan Basin: Geological Society of America Bulletin, v. 79, p. 827–854.

Lazar, O.R., Bohacs, K.M., Schieber, J., Macquaker, J.H.S., Demko, T. M., 2015, Mudstone Primer: Lithofacies variations, diagnostic criteria, and sedimentologic–stratigraphic implications at lamina to bedset scale: SEPM Society for Sedimentary Geology.

Li, Z., J. Bhattacharya, and J. Schieber, 2015, Evaluating along-strike variation using thin-bedded facies analysis, Upper Cretaceous Ferron Notom Delta, Utah: Sedimentology, v. 62, p. 2060–2089.

Lock, B. E., R. W. Butler, and R. T. Franklund, 2009, Tempestite Sedimentation : An Example from the Del Rio Formation of West Texas: GCAGS Transactions, v. 59, p. 463–476.

Lowe, D. R., 1982, Sediment Gravity Flows: II. Depositional Models With Special Reference To The Deposits Of High-Density Turbidity Currents: Journal of Sedimentary Petrology, v. 52, no. 1, p. 279–297.

MacEachern, J. A., K. L. Bann, J. P. Bhattacharya, and C. D. Howell Jr., 2005, Ichnology of deltas: Organism responses to the dynamic interplay of rivers, waves, storms, and tides: 49-85 p.

Macquaker, J. H. S., S. J. Bentley, and K. M. Bohacs, 2010, Wave-enhanced sediment-gravity flows and mud dispersal across continental shelves: Reappraising sediment transport processes operating in ancient mudstone successions: Geology, v. 38, no. 10, p. 947–950.

Milliman, J. D., and J. P. M. Syvitski, 1992, Geomorphic/Tectonic Control of Sediment Discharge to the Ocean: The Importance of Small Mountainous Rivers: The Journal of Geology, v. 100, no. 5, p. 525–544.

Molenaar, C. M., 1973, Sedimentary Facies and Correlation of the Gallup Sandstone and Associated Formations, Northwestern New Mexico: Cretaceous and Tertiary Rocks of the Southern Colorado Plateau, no. 1972, p. 85–110.

Molenaar, C. M., 1977, Stratigraphy and depositional history of Upper Cretaceous rocks of the San Juan Basin area, New Mexico and Colorado, with a note on economic resources: New Mexico Geological Society Guidebook, 28th Field Conference, San Juan Basin, v. 3, p. 159–166.

Mulder, T., and J. Alexander, 2001, The physical character of subaqueous sedimentary density flows and their deposits: Sedimentology, v. 48, p. 269–299.

Mulder, T., S. Migeon, B. Savoye, and J. C. Faugères, 2001, Inversely graded turbidite sequences in the deep Mediterranean: A record of deposits from flood-generated turbidity currents? Geo-Marine Letters, v. 21, no. 2, p. 86–93.

Mulder, T., J. P. M. Syvitski, S. Migeon, J. C. Faugères, and B. Savoye, 2003, Marine hyperpycnal flows: Initiation, behavior and related deposits. A review: Marine and Petroleum Geology, v. 20, no. 6–8, p. 861–882.

Myrow, P. M., W. Fischer, and J. W. Goodge, 2002, Wave-modified turbidites: combined-flow shoreline and shelf deposits, Cambrian, Antarctica: Journal of Sedimentary research, v. 72, no. 5, p. 641–656.

Nemec, W., 1995, The dynamics of deltaic suspension plumes, *in* M. N. Oti, and G. Postma, eds., Geology of Deltas: Rotterdam, A.A. Balkema, p. 31–93.

Nio, S.-D., and C.-S. Yang, 1991, Diagnostic attributes of clastic tidal deposits: a review, *in* D. G. Smith, G. E. Reinson, B. A. Zaitlin, and R. A. Rahmani, eds., Clastic Tidal Sedimentology: Canadian Society of Petroleum Geologists, Memoir 16: p. 3–28.

Nittrouer, C. a., S. a. Kuehl, A. G. Figueiredo, M. a. Allison, C. K. Sommerfield, J. M. Rine, L. E. C. Faria, and O. M. Silveira, 1996, The geological record preserved by Amazon shelf sedimentation: Continental Shelf Research, v. 16, no. 5–6, p. 817–841.

Normark, W. R., and D. J. W. Piper, 1991, Initiation Processes and Flow Evolution of Turbidity Currents: Implications for the Depositional Record: Tulsa, v. 46, p. 207–230.

Nummedal, D., and C. M. Molenaar, 1995, Sequence stratigraphy of ramp-setting strand plain successions: the Gallup Sandstone, New Mexico, *in* Sequences Stratigraphy of Foreland Basin Deposits: p. 277–310.

Passey, Q. R., K. E. Dahlberg, K. Sullivan, H. Yin, B. Brackett, Y. Xiao, and A. G. Guzman-Garcia, 2006, Definitions and Geological Occurence of Thin Beds in Clastics: AAPG Archie Series, v. 1, p. 26–39.

Pattison, S. a. J., 2005, Storm-Influenced Prodelta Turbidite Complex in the Lower Kenilworth Member at Hatch Mesa, Book Cliffs, Utah, U.S.A.: Implications for Shallow Marine Facies Models: Journal of Sedimentary Research, v. 75, no. 3, p. 420–439.

Pemberton, S. G., J. A. MacEachern, M. K. Gingras, and T. D. A. Saunders, 2008, Biogenic chaos: Cryptobioturbation and the work of sedimentologically friendly organisms: Palaeogeography, Palaeoclimatology, Palaeoecology, v. 270, no. 3–4, p. 273–279.

Piper, D. J. W., 1978, Turbidites, muds and silts on deep-sea fans and abyssal plains, *in* D. J. Stanley, and G. Kelling, eds., Sedimentation in Submarine Canyons, Fans, and Trenches: Dowden, Hutchinson and Ross, p. 163–176.

Plint, A. G., 2014, Mud dispersal across a Cretaceous prodelta: Storm-generated, wave-enhanced sediment gravity flows inferred from mudstone microtexture and microfacies: Sedimentology, v. 61, p. 609–647.

Plint, A. G., J. H. S. Macquaker, and B. L. Varban, 2012, Bedload Transport of Mud Across A Wide, Storm-Influenced Ramp: Cenomanian-Turonian Kaskapau Formation, Western Canada Foreland Basin: Journal of Sedimentary Research, v. 82, no. 11, p. 801–822.

Reineck, H.-E., and I. B. Singh, 1973, Current and Wave Ripples, *in* Depositional Sedimentary Environments: Berlin, Heidelberg, Springer Berlin Heidelberg, p. 14–47.

Ridgley, J. L., S. M. Condon, and J. R. Hatch, 2013, Geology and Oil and Gas Assessment of the Mancos-Menefee Composite Total Petroleum System Total Petroleum Systems and Geologic Assessment of Province , Exclusive of Paleozoic Rocks , New Mexico: U.S. Geologicial Survey Digital Data Series DDS–69–F, no. DDS-69-F, p. 1–207.

Sageman, B. B., and M. A. Arthur, 1994, Early Turonian Paleogeographic/Paleobathymetric Map, Western Interior, US: p. 457–469.

Schieber, J., 2016, Mud re-distribution in epicontinental basins - Exploring likely processes: Marine and Petroleum Geology, v. 71, p. 119–133.

Schieber, J., 2003, Simple Gifts and Buried Treasures-Implications of Finding Bioturbationo and Erosion Surfaces in Black Shales: The Sedimentary Record, v. 1, no. 2, p. 4–8.

Suter, J. R., 2006, Facies Models Revisited: Clastic Shelves: 339-397 p.

Talling, P. J., D. G. Masson, E. J. Sumner, and G. Malgesini, 2012, Subaqueous sediment density flows: Depositional processes and deposit types: Sedimentology, v. 59, no. 7, p. 1937–2003.

Taylor, A. M., and R. Goldring, 1993, Description and analysis of bioturbation and ichnofabric: Journal of the Geological Society, v. 150, no. 1, p. 141–148.

Traykovski, P., W. R. Geyer, J. D. Irish, and J. F. Lynch, 2000, The role of wave-induced density-driven fluid mud flows for cross-shelf transport on the Eel River continental shelf: Continental Shelf Research, v. 20, no. 16, p. 2113–2140.

Weatherford Laboratories, 2010, San Juan 28-6 Ut 148M well Rio Arriba County, New Mexico- Core Analysis Report: Appendix D p.

Wheatcroft, R. A., 2000, Oceanic flood sedimentation: A new perspective: Continental Shelf Research, v. 20, no. 16, p. 2059–2066.